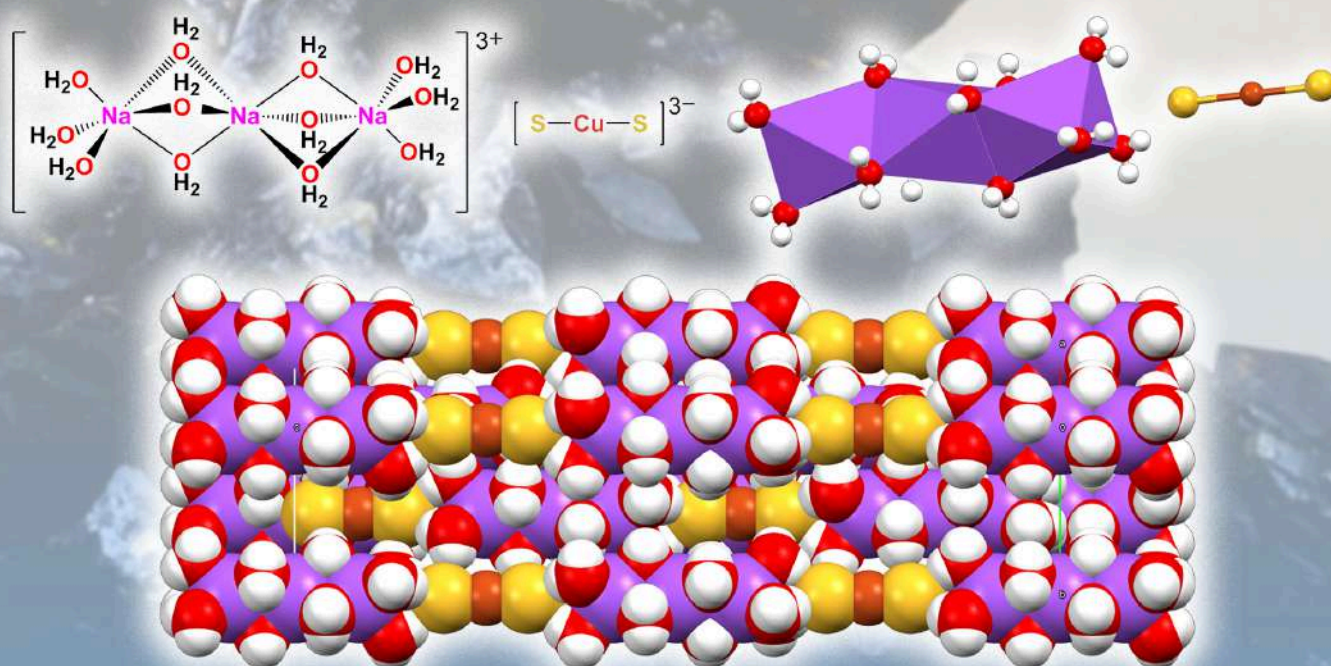




Sodium Dithiocuprate(I) Dodecahydrate—A “Passport Photo” of the $[\text{CuS}_2]^{3-}$ Anion

Volume 15 · Issue 6 June 2025



Search for Articles:

Search

Advanced

Journals / Crystals / Editorial Board

IMPACT FACTOR 2.4

CITESCORE 5.0



Submit to Crystals

Review for Crystals

Journal Menu

- Crystals Home
- Aims & Scope
- Editorial Board
- Reviewer Board
- Topical Advisory Panel
- Instructions for Authors
- Special Issues
- Topics
- Sections & Collections
- Article Processing Charge
- Indexing & Archiving
- Editor's Choice Articles
- Most Cited & Viewed
- Journal Statistics
- Journal History
- Journal Awards
- Society Collaborations
- Conferences
- Editorial Office

Journal Browser

Volume

Issue

Go

- > Forthcoming issue
- > Current issue

Vol. 15 (2025)	Vol. 7 (2017)
Vol. 14 (2024)	Vol. 6 (2016)
Vol. 13 (2023)	Vol. 5 (2015)
Vol. 12 (2022)	Vol. 4 (2014)
Vol. 11 (2021)	Vol. 3 (2013)
Vol. 10 (2020)	Vol. 2 (2012)
Vol. 9 (2019)	Vol. 1 (2011)
Vol. 8 (2018)	

Special Issue
Advanced Materials for CO₂ Reduction

Guest Editor
Dr. Dany Sun

Deadline
29 October 2025

Editorial Board

- Liquid Crystals Section
- Biomolecular Crystals Section
- Crystal Engineering Section
- Industrial Crystallization Section
- Inorganic Crystalline Materials Section
- Organic Crystalline Materials Section
- Macromolecular Crystals Section
- Mineralogical Crystallography and Biomimetic Section
- Hybrid and Composite Crystalline Materials Section
- Materials for Energy Applications Section
- Crystalline Metals and Alloys Section
- Polycrystalline Ceramics Section

Please note that the order in which the Editors appear on this page is alphabetical, and follows the structure of the editorial board presented on the MDPI website under information for editors, editorial board responsibilities.

Members



Prof. Dr. Alessandra Iaconis [Website](#)
Section Editor-in-Chief

Department of Physics, University of Pisa, 56126 Pisa, PI, Italy
Interests: photonics; rare-earth luminescence; optical spectroscopy; THz spectroscopy; crystal growth
Special Issues, Collections and Topics in MDPI journals



Prof. Dr. Hongbin Bai [Website](#)
Section Editor-in-Chief

School of Materials Science and Engineering, Zhejiang University, Hangzhou 310000, China
Interests: alloy design and behavior; structural materials under extreme conditions; multiscale mechanical behaviors; physical metallurgy; metal and alloys; single crystals; plasticity
Section: Crystalline Metals and Alloys
Special Issues, Collections and Topics in MDPI journals



Prof. Dr. Vladimir Chepurov [Website](#)
Section Editor-in-Chief

Department of Electronic, Computer Engineering, Hong Kong University of Science and Technology, Hong Kong, China
Interests: liquid crystals; electrooptics; displays; photonics; photocalignment; photopatterning
Section: Liquid Crystals
Special Issues, Collections and Topics in MDPI journals



Dr. José Gavira [Website](#)
Section Editor-in-Chief

IACT (CSIC-UGR), Avilés, Spain
Interests: protein crystallization: nucleation, growth and crystals quality; protein crystallography; protein crystals biocomposites and properties; enzymatic crystals (CLEC)
Section: Biomolecular Crystals
Special Issues, Collections and Topics in MDPI journals



Prof. Dr. Leonid Kuzlov [Website](#)
Section Editor-in-Chief

1. N.O. Zaitzky Institute of Organic Chemistry, Russian Academy of Sciences, Leninsky Prospekt 47, 119991 Moscow, Russia
2. Chemistry Department, Moscow State University, Leninskie Gory 1, Bldg. 3, 119992 Moscow, Russia
3. Institute of Ecology and Engineering, National Science and Technology University MISIS, Leninsky Prospekt 4, 119071 Moscow, Russia
Interests: catalysis; nanomaterials; renewables; green chemistry
Section: Hybrid and Composite Crystalline Materials
Special Issues, Collections and Topics in MDPI journals



Prof. Dr. Heike Lorenz [Website](#)
Section Editor-in-Chief

Max Planck Institute for Dynamics of Complex Technical Systems, 39106 Magdeburg, Germany
Interests: phase equilibria; crystallization kinetics; process monitoring & design; separation of fine chemicals; large scale industrial products and renewable resources; innovative crystallization-based separation concepts; emulsions; natural products; multi-component mixtures
Section: Industrial Crystallization
Special Issues, Collections and Topics in MDPI journals

Search for Articles:

Search

Advanced

Journals / Crystals / Reviewer Board



Submit to Crystals

Review for Crystals

Journal Menu

- [Crystals Home](#)
- [Aims & Scope](#)
- [Editorial Board](#)
- [Reviewer Board](#)
- [Topical Advisory Panel](#)
- [Instructions for Authors](#)
- [Special Issues](#)
- [Topics](#)
- [Sections & Collections](#)
- [Article Processing Charge](#)
- [Indexing & Archiving](#)
- [Editor's Choice Articles](#)
- [Most Cited & Viewed](#)
- [Journal Statistics](#)
- [Journal History](#)
- [Journal Awards](#)
- [Society Collaborations](#)
- [Conferences](#)
- [Editorial Office](#)

Journal Browser

Volume

Issue

- [Forthcoming issue](#)
- [Current issue](#)

Vol. 15 (2025)	Vol. 7 (2017)
Vol. 14 (2024)	Vol. 6 (2016)
Vol. 13 (2023)	Vol. 5 (2015)
Vol. 12 (2022)	Vol. 4 (2014)
Vol. 11 (2021)	Vol. 3 (2013)
Vol. 10 (2020)	Vol. 2 (2012)
Vol. 9 (2019)	Vol. 1 (2011)
Vol. 8 (2018)	



2024 Reviewer Acknowledgment

Thank you
for your contribution!Join us:
[mdpi.com/
reviewers](https://mdpi.com/reviewers)IMPACT
FACTOR
2.4CITESCORE
5.0

Reviewer Board

Members of the reviewer board are selected from all **Crystals** reviewers for regularly providing timely high quality reports on submitted manuscripts. The possibilities of reviewer are available [here](#).

Members

Dr. Pavel Abramov [Website](#)

Nikolov Institute of Inorganic Chemistry SB RAS, 3 Akad. Lomonosov Ave., 63000 Novosibirsk, Russia
Interests: polycrystalline, inorganic materials

Dr. Agnieszka Adamczyk-Wozniak [Website](#)

Faculty of Chemistry, Warsaw University of Technology, 3 Noakowskiego Street, 00-864 Warsaw, Poland
Interests: phanylboronic compounds, spectroscopy, characterization, organic synthesis, metalloorganic synthesis

Prof. Dr. Chinyere A. Adetayo

Department of Physics, Federal Univ. of Agriculture, Abeokuta, Nigeria

Interests: condensed matter physics, materials science, molecular dynamics simulation, density functional theory, electronic structure calculations, band structure, thermoelectric, perovskites

Dr. Pedro Matejo Alcalde [Website](#)

Universidad Complutense de Madrid, Dpto. Física de Materiales, Fac. Ciencias Físicas-UCM, Ciudad Universitaria s/n, Madrid, Spain

Interests: nanomaterials growth and characterization, transparent conductive oxides, optoelectronic properties, Electron Microscopy, optical spectroscopy

Dr. Sara Amorim [Website](#)

1. 3B's Research Group, ICB – Research Institute on Biomaterials, Biodegradables and Biomimetics, University of Minho, Headquarters of the European Institute of Excellence on Tissue Engineering and Regenerative Medicine, Av. Park, Parque de Ciência e Tecnologia, Zona Industrial de Gandra, 4805-017 Barco, Guimarães, Portugal

2. ICVS/3B's-PT Government Associate Laboratory, Braga, 4805-017 Guimarães, Portugal
Interests: layer-by-layer assembly, qm-c-SiN, biomimetics, glycoantimicrobial

Dr. Emmanuel Amm-Damo [Website](#)

Crystalline Group, Solvay Specialty Polymers, Alpharetta, USA

Interests: order, crystal structure, freezing, Anti-icing materials, polymers, composites, thermal properties, thermal conductivity, thin films, structural properties relationships, spectroscopy

Open Access Review

36 pages, 5287 KiB 

Preparation, Properties, and Applications of 2D Janus Transition Metal Dichalcogenides

by Haoyang Zhao and Jeffrey Chor Keung Lam

Crystals 2025, 15(6), 567; <https://doi.org/10.3390/cryst15060567> - 16 Jun 2025

Viewed by 177

Abstract Structural symmetry significantly influences the fundamental characteristics of two-dimensional (2D) materials. In conventional transition metal dichalcogenides (TMDs), the absence of in-plane symmetry introduces distinct optoelectronic behaviors. To further enrich the functionality of such materials, recent efforts have focused on disrupting out-of-plane symmetry—often through [...] [Read more.](#)

(This article belongs to the Special Issue Structural Engineering of Low-Dimensional Materials for Desired Properties)

► [Show Figures](#)

Open Access Article

14 pages, 2451 KiB 

Mechanical and Electronic Properties of Fe(II) Doped Calcite: Ab Initio Calculations

by Zhangci Wu, Xiao Zhi, Fujie Jia, Jiayuan Ye and Neng Li

Crystals 2025, 15(6), 568; <https://doi.org/10.3390/cryst15060568> - 16 Jun 2025

Viewed by 104

Abstract Calcite (CaCO_3), a widely used mineral in materials science and environmental engineering, exhibits excellent stability but has limited mechanical strength and a wide electronic band gap, restricting its broader functional applications. To address these limitations, we systematically investigated the effects of [...] [Read more.](#)

(This article belongs to the Special Issue Design and Synthesis of Functional Crystal Materials)

► [Show Figures](#)

Open Access Article

16 pages, 2624 KiB 

Grain Size Engineering and Tuning of Magnetic Properties in Ultra-Thin NiMnGa Glass-Coated Microwires: Insights from Annealing Effects

by Mohamed Salaheldeen, Valentina Zhukova, Julian Gonzalez and Arcady Zhukov

Crystals 2025, 15(6), 565; <https://doi.org/10.3390/cryst15060565> - 16 Jun 2025

Viewed by 131

Abstract We studied the influence of annealing on the magnetic properties and microstructure of ultrathin (metallic nucleus diameter $\approx 5 \mu\text{m}$, total diameter $\approx 19 \mu\text{m}$) Heusler-type NiMnGa glass-coated microwires prepared using the Taylor–Ulitsky method. The as-prepared NiMnGa microwires exhibit unexpectedly strong magnetic anisotropy, [...] [Read more.](#)

(This article belongs to the Special Issue Recent Advances in Microstructure and Properties of Metals and Alloys)

► [Show Figures](#)

Open Access Article

15 pages, 2028 KiB 

Physicochemical Properties of Demineralized Bone Matrix and Calcium Hydroxide Composites Used as Bone Graft Material

by Octarina, Florencia Livia Kurniawan, Firda Amalia Larosa, Olivia Nauli Komala and Meircurius Dwi Condro Surboyo

Crystals 2025, 15(6), 564; <https://doi.org/10.3390/cryst15060564> - 15 Jun 2025

Viewed by 213

Abstract Vertical bone defects can result in alveolar bone resorption, which may be addressed using composite grafts. A combination of demineralized bone matrix (DBM) and calcium hydroxide (Ca(OH)_2) has potential as a bone substitute due to its biological and structural properties. This [...] [Read more.](#)

► [Show Figures](#)

Article

Physicochemical Properties of Demineralized Bone Matrix and Calcium Hydroxide Composites Used as Bone Graft Material

Octarina ¹, Florencia Livia Kurniawan ^{1,*}, Firda Amalia Larosa ¹, Olivia Nauli Komala ²
and Meircurius Dwi Condro Surboyo ³

¹ Department of Dental Material, Faculty of Dentistry Universitas Trisakti, Jakarta 11440, Indonesia; octarina@trisakti.ac.id (O.); famalia02@gmail.com (F.A.L.)

² Department of Periodontics, Faculty of Dentistry Universitas Trisakti, Jakarta 11440, Indonesia; olivia.nauli@trisakti.ac.id

³ Department of Oral Medicibe, Faculty of Dental Medicine, Universitas Airlangga, Surabaya 60132, Indonesia; meircurius-2015@fkg.unair.ac.id

* Correspondence: florencia@trisakti.ac.id

Abstract: Vertical bone defects can result in alveolar bone resorption, which may be addressed using composite grafts. A combination of demineralized bone matrix (DBM) and calcium hydroxide (Ca(OH)₂) has potential as a bone substitute due to its biological and structural properties. This study aimed to identify the optimal DBM–Ca(OH)₂ ratio by evaluating their physicochemical properties relevant to bone regeneration. DBM gel and Ca(OH)₂ powder were combined at ratios of 1:1, 2:1, 3:1, and 4:1. The mixtures were freeze-dried, ground, and sieved to create granules. The composites were analyzed in terms of their structural and chemical characteristics, including crystallinity, calcium ion release, functional group composition, particle size, surface morphology, and elemental distribution. Increasing the proportion of DBM reduced crystallinity and calcium ion release while influencing particle size. Among all groups, the 2:1 composite demonstrated the most balanced properties: moderate crystallinity, relatively high calcium release, and favorable particle size. Chemical analyses confirmed the presence and interaction of both organic and inorganic components, while elemental mapping showed a uniform distribution of the key elements essential for bone formation. The DBM–Ca(OH)₂ composite at a 2:1 ratio has the most promising physicochemical profile, making it a strong candidate for bone graft applications. However, a limitation of this study is the absence of biological testing. Future research should investigate the in vitro and in vivo performance of this composite in bone regeneration.



Academic Editor: Michele Iafisco

Received: 16 April 2025

Revised: 3 June 2025

Accepted: 9 June 2025

Published: 15 June 2025

Citation: Octarina; Kurniawan, F.L.; Larosa, F.A.; Komala, O.N.; Surboyo, M.D.C. Physicochemical Properties of Demineralized Bone Matrix and Calcium Hydroxide Composites Used as Bone Graft Material. *Crystals* **2025**, *15*, 564. <https://doi.org/10.3390/cryst15060564>

Copyright: © 2025 by the authors. Licensee MDPI, Basel, Switzerland. This article is an open access article distributed under the terms and conditions of the Creative Commons Attribution (CC BY) license (<https://creativecommons.org/licenses/by/4.0/>).

Keywords: bone graft; demineralized bone matrix; calcium hydroxide; crystallinity; solubility; functional groups; surface morphology

1. Introduction

Vertical bone defects, characterized by bone loss extending below the alveolar crest, can lead to significant alveolar bone resorption, often requiring a periodontal surgical intervention to restore bone integrity [1,2]. Periodontal flap surgery aims to remove damaged tissue and promote healing and is often supported by bone grafts that serve as scaffolds to stimulate new bone growth and repair defects [3,4]. Optimizing these graft materials is crucial to improving outcomes in periodontal therapy, especially for complex bone loss, where it may help avoid dental procedures such as denture placement [5,6].

Demineralized bone matrix (DBM), derived from bovine bone, undergoes demineralization to remove organic components and retain inorganic components—especially

hydroxyapatite ($\text{Ca}_{10}(\text{PO}_4)_6(\text{OH})_2$)—reducing its crystallinity and mimicking the composition of human bone. DBM contains collagen, non-collagenous proteins, and growth factors like bone morphogenetic proteins (BMPs) and transforming growth factor-beta (TGF- β) [7,8], which contribute to its osteoinductive properties by promoting osteogenic differentiation and bone formation [9,10]. Its collagen matrix provides an osteoconductive scaffold that supports cell attachment and proliferation during bone healing [11,12]. However, demineralization lowers its calcium content, making supplementation necessary to enhance DBM's bone-forming potential [13].

Calcium hydroxide ($\text{Ca}(\text{OH})_2$) supplies osteoinductive calcium ions, encourages hard tissue formation, possesses antibacterial properties due to its alkalinity, and stimulates angiogenesis through growth factor release [14–16]. Combining DBM with $\text{Ca}(\text{OH})_2$ has been shown to improve osteoinductive activity, supporting osteoblast proliferation and mineralization [14]. Composite grafts containing these materials can harness both osteoconductive and osteoinductive effects, improving bone regeneration [17]. Granular DBM- $\text{Ca}(\text{OH})_2$ composites at ratios of 1:1, 2:1, 3:1, and 4:1 were developed, offering favorable structure, morphology, and clinical handling [18,19].

Physicochemical characteristics, such as crystallinity, calcium content, chemical bonding, and surface morphology, directly influence graft performance and bone regeneration potential [20–22]. Although previous studies have explored the individual use and combined application of DBM and $\text{Ca}(\text{OH})_2$, comprehensive data on the composite's physicochemical properties, especially in granular form, remain limited. There is a lack of detailed characterization used to determine how varying DBM- $\text{Ca}(\text{OH})_2$ ratios affect key parameters essential for bone graft efficacy. To address this gap, the present study uses X-ray diffraction (XRD) to evaluate the composite's crystallinity and phase composition [23–25]; Atomic Absorption Spectroscopy (AAS) to quantify its calcium ion concentration and solubility [26]; Fourier Transform Infrared Spectroscopy (FTIR) to identify functional groups and chemical interactions [27]; and Scanning Electron Microscopy with Energy-Dispersive X-ray Spectroscopy (SEM-EDS) to analyze its surface morphology, particle size, and elemental distribution [28]. This approach aims to identify the optimal DBM- $\text{Ca}(\text{OH})_2$ ratio with physicochemical properties suitable for further biological evaluation as a bone graft material.

Understanding these properties is essential as crystallinity influences biodegradability and osteoblast adhesion, solubility relates to material degradation and bone remodeling balance, and surface morphology and elemental composition impact cell attachment and osteoconductivity [29]. Although both DBM and $\text{Ca}(\text{OH})_2$ possess osteoinductive potential, the optimal physicochemical balance for bone regeneration has not been clearly established. It is hypothesized that increasing the proportion of DBM in the DBM- $\text{Ca}(\text{OH})_2$ composite will result in a lower overall crystallinity due to the amorphous nature of the demineralized matrix, which lacks ordered mineral phases. Additionally, despite undergoing demineralization, the DBM retains residual calcium and may facilitate greater calcium ion release through its organic matrix, potentially leading to higher detectable calcium concentrations than $\text{Ca}(\text{OH})_2$ alone. This unique combination may enhance ion availability and elemental distribution, improving the material's potential for bone grafting applications. Therefore, it is hypothesized that a DBM-rich composite will demonstrate a favorable crystallinity, calcium ion availability, and surface morphology, making it a promising candidate for further bone regeneration studies. This study aims to determine the optimal ratio of DBM- $\text{Ca}(\text{OH})_2$ (1:1, 2:1, 3:1, 4:1) in composite grafts by analyzing various physicochemical parameters, like crystallinity, solubility, functional groups, and surface morphology, in order to evaluate their potential suitability as bone graft materials.

2. Materials and Methods

2.1. Fabrication of DBM-Ca(OH)₂

Cortical bovine bone was obtained from a licensed slaughterhouse in Surabaya, East Java. The bone was cut into small sections and thoroughly cleaned using hydrogen peroxide (H₂O₂) to remove surface contaminants. To defat the bone, samples were immersed in an ultrasonic shaker kept at 60 °C until they appeared white and free of fatty tissue. The defatted bone was rinsed 3–4 times with distilled water to remove any residual peroxide and reduce toxicity.

The cleaned bone was demineralized by immersion in 1% hydrochloric acid (HCl), which removed the inorganic material while preserving the organic matrix. Following demineralization, the samples were rinsed 3–4 times with distilled water to eliminate residual acid. The demineralized bone was then mixed with 0.9% sodium chloride (NaCl) solution in a 1:1 ratio and homogenized using a blender to produce DBM gel.

Composite preparation was performed at the Tissue Bank, Dr. Soetomo Hospital, Surabaya, East Java. DBM gel and calcium hydroxide (Ca(OH)₂) powder (Merck, Darmstadt, Germany) were combined at four different weight ratios: 1:1, 2:1, 3:1, and 4:1. Each mixture was homogenized using a magnetic stirrer until a uniform consistency was achieved.

The homogenized mixtures were poured into 10 cm diameter Petri dishes and frozen at −80 °C for 24 h. Freeze-drying was conducted for 48 h at −100 °C to obtain a dry composite. The dried samples were then ground using a bone miller and sieved through a mesh (>710 μm) to obtain uniform granules (Figure 1).



Figure 1. DBM-Ca(OH)₂ prepared to four different weight ratios: 1:1, 2:1, 3:1, and 4:1.

2.2. X-Ray Diffraction (XRD)

The sample, initially in granule form, was ground into a fine powder to ensure homogeneity and improve its diffraction quality. An total of 1 g of the powdered sample was prepared for each experimental group. X-ray diffraction (XRD) analysis was performed using CuK α radiation ($\lambda = 1.5406 \text{ \AA}$) with a scan range of 10° to 90° (2 θ) and a step size of 0.01°. The X-ray diffraction (XRD) peaks obtained from the analysis were compared with standard reference patterns of known crystal structures to identify the crystalline phases present in the sample [30]. This phase identification was carried out using “Match!” software 3.15 version, which utilizes crystallographic databases such as ICDD. Furthermore, the diffraction peak’s characteristics—including its intensity, position, and full width at half maximum (FWHM)—were used to evaluate the degree of crystallinity and estimate the crystallite size. The degree of crystallinity was quantified using “Origin 2024 (10.1)

version” software through peak deconvolution and area integration methods, providing insights into the structural ordering of the material.

2.3. Atomic Absorption Spectroscopy (AAS)

To assess their calcium ion release, 25 mg of each granulated DBM–Ca(OH)₂ sample was immersed in 25 mL of Tris-HCl buffer (pH 7.4) to simulate physiological conditions. The samples were incubated at 37 °C for 7 days. Post-incubation, the solutions were filtered using Whatman filter paper to remove particulates. The calcium ion concentration of the filtrate was then quantified using a Thermo Scientific iCE 3000 Series Atomic Absorption Spectrometer (AAS) Waltham City, Massachusetts, United States.

The AAS system operated with acetylene gas and an airflow adjusted to the recommended pressure settings. The instrument’s flame and hollow cathode lamp, which are specifically used for calcium, were activated, and the sample solutions were aspirated into the spray chamber. Measurements were taken at a wavelength of 422.7 nm, and calcium concentrations were recorded in mg/L.

2.4. Fourier Transform Infrared (FTIR) Spectroscopy

The sample, initially in granule form, was subjected to functional group analysis using an IR Prestige-21 FTIR spectrometer (Shimadzu, Japan). To enhance homogeneity, the granules were finely ground and thoroughly mixed with potassium bromide (KBr) and then pressed into transparent pellets to optimize their spectral resolution.

Measurements were performed using the Diffuse Reflectance-Fourier Transform Infrared Spectroscopy (DRS-FTIR) technique over a spectral range of 400–4000 cm^{−1}. The spectrometer operated at a resolution of 2.0 cm^{−1}, and each spectrum was averaged from 20 scans. Spectra were recorded as percent transmittance and analyzed to identify functional groups based on their characteristic absorption bands.

FTIR spectral data were compared with reference databases to determine functional group identities. Further analysis and visualization of absorption peaks were conducted using Origin software to support their interpretation and facilitate comparison.

2.5. Scanning Electron Microscope (SEM)—Energy-Dispersive X-Ray Spectroscopy (EDS)

Prior to imaging, the sample was mounted on a specimen holder and sputter-coated with a thin layer of gold–palladium to enhance its electrical conductivity and reduce charging effects. SEM imaging was performed under high-vacuum conditions using an accelerating voltage of 20 kV, a working distance of 9.9 mm, a magnification of 1000×, and a standard probe current of 25. The surface morphology of the samples was visualized and recorded using the SEM system. Subsequent image analysis, including particle size measurements and surface structure evaluations, was conducted using ImageJ 1.54i version software.

2.6. Statistical Analysis

Calcium ion concentration data obtained from the AAS analysis were evaluated using a one-way Analysis of Variance (ANOVA) and followed by a Bonferroni post hoc test to identify statistically significant differences among the DBM–Ca(OH)₂ ratio groups. Other characterization parameters (XRD, FTIR, SEM-EDS) were analyzed descriptively by presenting their mean values. All statistical analyses were performed using the Statistical Package for the Social Sciences (SPSS 30) software for Windows, with the significance level set at $p < 0.05$.

3. Results

3.1. X-Ray Diffraction (XRD)

Figure 2 displays the XRD patterns of Ca(OH)_2 , DBM, and DBM- Ca(OH)_2 composites with varying ratios (1:1, 2:1, 3:1, and 4:1). The XRD pattern of pure Ca(OH)_2 shows distinct diffraction peaks at 2θ values around 17.9° , 28.5° , 34.0° , 47.0° , 50.7° , 54.2° , 62.5° , 64.1° , 71.6° , and 84.6° , which are consistent with its known crystalline structure. These peaks were also observed in the DBM- Ca(OH)_2 composite groups, indicating the presence of crystalline calcium hydroxide in these mixtures.

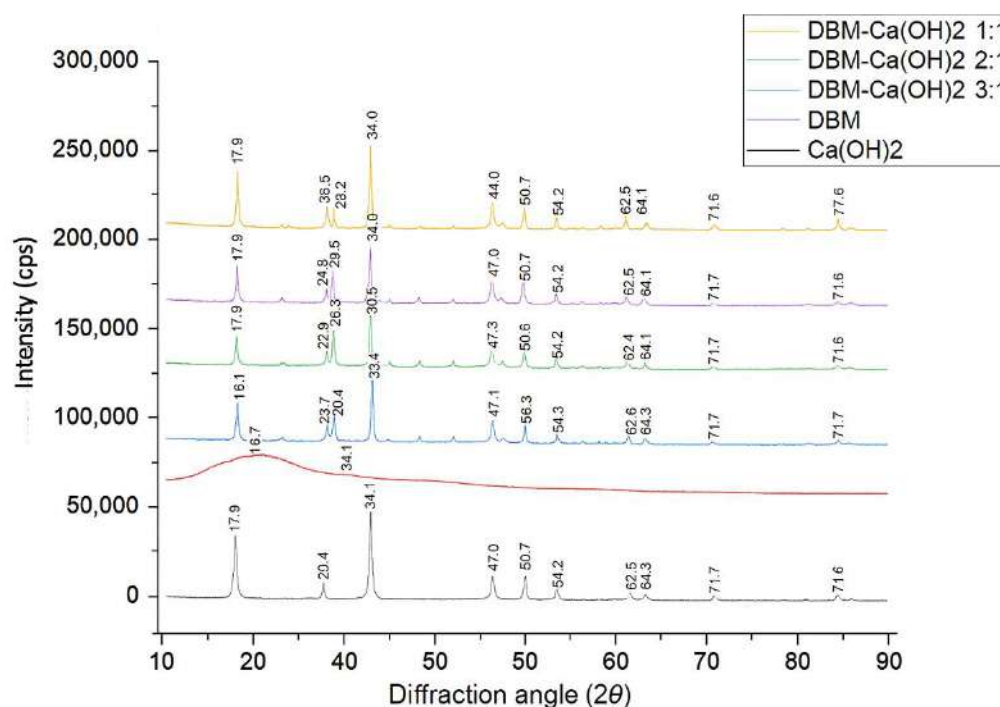


Figure 2. XRD spectra of DBM, Ca(OH)_2 , and DBM- Ca(OH)_2 composites in ratios of 1:1, 2:1, 3:1, 4:1.

The DBM sample exhibited an amorphous pattern with no distinct peaks, confirming the absence of crystalline phases after its demineralization. As the proportion of DBM increased (from 1:1 to 4:1), the intensity of the Ca(OH)_2 peaks gradually decreased, suggesting a reduced crystallinity due to dilution by the amorphous DBM.

Quantitative analysis of the degree of crystallinity showed the highest crystallinity in pure Ca(OH)_2 (63.1%), followed by DBM- Ca(OH)_2 at a 1:1 ratio (58.6%). The crystallinity progressively decreased to 48.1% in the 4:1 group (Table 1). These results indicate that increasing the DBM content attenuates the crystalline structure of Ca(OH)_2 in the composite, potentially enhancing the composite's bioresorbability and biological performance.

Table 1. Crystal phase and degree of crystallinity (%) of each sample, determined from XRD data.

Sample *	Crystal Phase	Degree of Crystallinity
DBM- Ca(OH)_2 1:1	Ca(OH)_2	58.6%
DBM- Ca(OH)_2 2:1	Ca(OH)_2	51.6%
DBM- Ca(OH)_2 3:1	Ca(OH)_2	48.5%
DBM- Ca(OH)_2 4:1	Ca(OH)_2	48.1%
DBM	-	-
Ca(OH)_2	Ca(OH)_2	63.1%

* One sample from each group was used for this test.

3.2. Atomic Absorption Spectroscopy (AAS)

The calcium ion release profile of Ca(OH)₂, DBM, and the DBM–Ca(OH)₂ composites was evaluated using AAS after 7 days of incubation in Tris-HCl buffer (pH 7.4). The results, presented in Table 2, show a clear trend: the calcium ion concentration decreased with increasing proportions of DBM in the composite.

Table 2. Calcium ion concentration (mg/L) of Ca(OH)₂, DBM, and DBM–Ca(OH)₂ composites, measured by AAS after 7 days of incubation in Tris-HCl buffer.

Sample	Number of Sample	Calcium Ion Concentration (mg/L) ($\bar{x} \pm SD$)	<i>p</i> -Value
DBM–Ca(OH) ₂ 1:1	3	218.56 ± 1.37	<0.001 *
DBM–Ca(OH) ₂ 2:1	3	214.71 ± 1.53	
DBM–Ca(OH) ₂ 3:1	3	209.65 ± 0.80	
DBM–Ca(OH) ₂ 4:1	3	205.11 ± 0.99	
DBM	3	2.31 ± 0.32	
Ca(OH) ₂	3	229.60 ± 1.94	

* There is a significant difference in the one-way ANOVA ($p < 0.05$).

The largest calcium ion release was observed in pure Ca(OH)₂ (229.60 ± 1.94 mg/L), followed by DBM–Ca(OH)₂ composites in decreasing order: 1:1 (218.56 ± 1.37 mg/L), 2:1 (214.71 ± 1.53 mg/L), 3:1 (209.65 ± 0.80 mg/L), and 4:1 (205.11 ± 0.99 mg/L). DBM alone released a minimal amount of calcium ions (2.31 ± 0.32 mg/L), confirming its demineralized state.

The one-way ANOVA revealed a statistically significant difference in calcium ion concentration among the groups ($p < 0.001$), with the DBM–Ca(OH)₂ 4:1 group showing the lowest calcium release among the composites. This suggests that increasing the proportion of DBM dilutes the calcium content of the composite and reduces its ion release capacity.

3.3. Fourier Transform Infrared (FTIR) Spectroscopy

The FTIR spectra of DBM, Ca(OH)₂, and the DBM–Ca(OH)₂ composites at ratios of 1:1, 2:1, 3:1, and 4:1 are shown in Figure 3 and Table 3. These spectra illustrate the characteristic functional groups of each material and confirm the presence of both organic and inorganic phases in the composites. In the DBM sample, the following characteristic peaks of collagen were observed:

- Amide A (N–H stretching) at 3595 cm^{−1};
- Amide B (C–H stretching) at 2924 cm^{−1};
- Amide I (C=O stretching) at 1634 cm^{−1};
- Amide II (N–H bending) at 1547 cm^{−1};
- Amide III (C–N stretching) at 1240 cm^{−1};
- OH[−] at 3300 cm^{−1}.

The Ca(OH)₂ sample exhibited OH[−] stretching at 3641 cm^{−1}; CO₃^{2−} peak at 1463 cm^{−1}.

In the DBM–Ca(OH)₂ composites, notable new absorption bands confirmed the successful integration of inorganic content:

- PO₄^{3−} was detected at ~1056 cm^{−1} (1057 cm^{−1} in 3:1 group);
- COO[−] bands were observed in the ranges of 1407–1417 cm^{−1} and 1641–1648 cm^{−1} across all composite groups, suggesting ionic interaction between Ca²⁺ and the carboxyl groups in collagen;
- OH[−] stretching was present at 3638–3639 cm^{−1} in all composites.

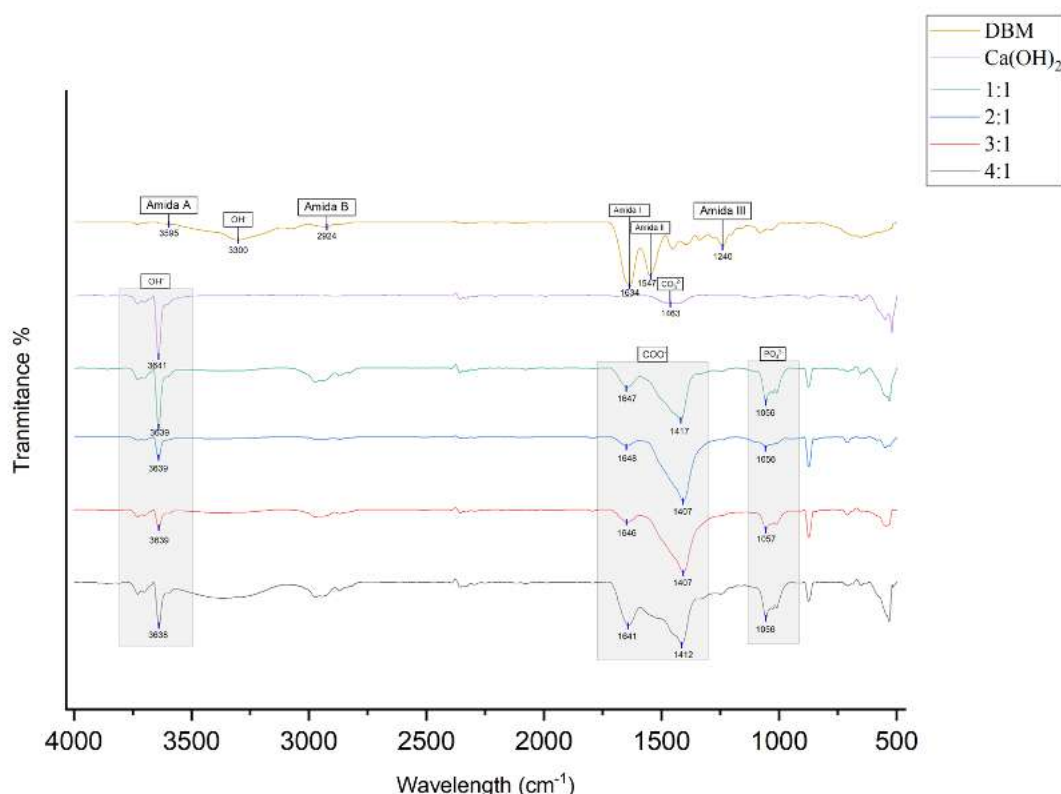


Figure 3. FTIR results for DBM, $\text{Ca}(\text{OH})_2$, and $\text{DBM-Ca}(\text{OH})_2$ in ratios of 1:1, 2:1, 3:1, and 4:1. One sample from each group was used for this test.

Table 3. Absorption peaks of functional groups from the amide I, amide II, amide III, amide A, amide B, phosphate (PO_4^{3-}), carbonate (CO_3^{2-}), carboxylate (COO^-), and hydroxyl (OH^-) groups were detected.

Compound	Functional Group	Infrared Wavelength
Amide I	Stretching C=O	1600–1700 cm^{-1}
Amide II	Stretching C-N Bending N-H	1480–1575 cm^{-1}
Amide III	Stretching C-N Bending N-H	1200–1300 cm^{-1}
Amide A	Stretching N-H	3300–3500 cm^{-1}
Amide B	Stretching N-H	2900–3100 cm^{-1}
PO_4^{3-}	Asymmetry Stretching P-O	1030–1090 cm^{-1}
CO_3^{2-}	Asymmetry Stretching C-O	1400–1500 cm^{-1}
COO^-	Symmetry Stretching C-O-O Asymmetry Stretching C-O-O	1300–1420 cm^{-1} 1550–1650 cm^{-1}
OH^-	Stretching O-H	3300–3650 cm^{-1}

Characteristic collagen peaks from DBM (amide groups and hydroxyl) and mineral peaks from $\text{Ca}(\text{OH})_2$ (hydroxyl and carbonate) are present in the composites, indicating the retention of both phases. Importantly, the appearance of phosphate (PO_4^{3-}) and carboxylate (COO^-) bands, along with shifts in hydroxyl stretching frequencies, demonstrates that chemical bonding and ionic interactions occur between the calcium ions and collagen carboxyl groups. These spectral changes suggest the formation of a bone-like apatite structure within the composite, which likely enhances its osteoconductive potential and suitability for bone regeneration applications.

3.4. Scanning Electron Microscope (SEM)—Energy-Dispersive X-Ray Spectroscopy (EDS)

The SEM micrographs of DBM, $\text{Ca}(\text{OH})_2$, and the DBM- $\text{Ca}(\text{OH})_2$ composites with ratios of 1:1, 2:1, 3:1, and 4:1 are presented in Figure 4. Their visual appearance reveals the morphological differences among the samples, with $\text{Ca}(\text{OH})_2$ particles exhibiting a broad size distribution. The DBM particles, being primarily organic, did not display distinct particulate features suitable for size measurements.

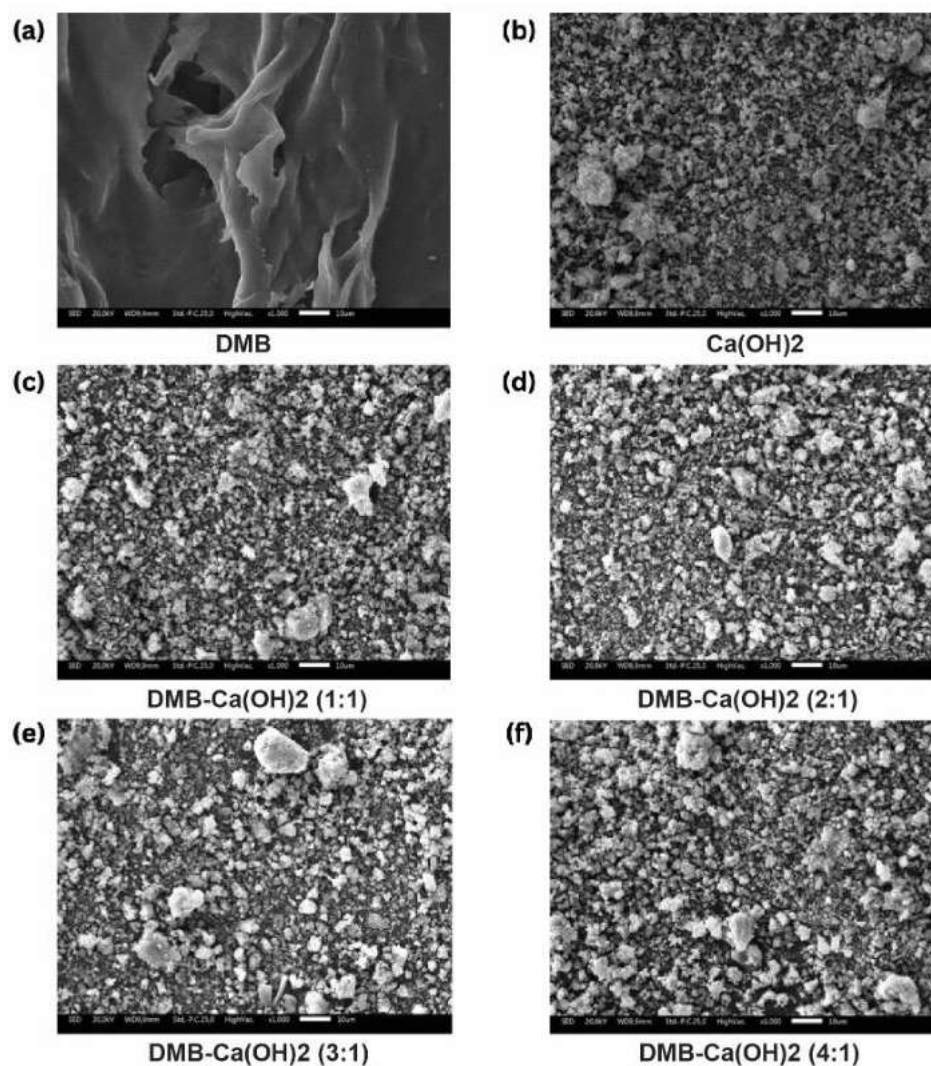


Figure 4. (a–f) The morphological characteristics of DBM- $\text{Ca}(\text{OH})_2$ (1000 \times magnification).

The $\text{Ca}(\text{OH})_2$ particles ranged from 0.01 μm to 350.68 μm in size, with an average particle size of $6.34 \pm 29.56 \mu\text{m}$. The incorporation of DBM into the composites reduced the maximum particle size and average particle size compared to pure $\text{Ca}(\text{OH})_2$. Specifically, average particle sizes decreased to $4.37 \pm 13.42 \mu\text{m}$ for the 1:1 ratio, $4.50 \pm 13.28 \mu\text{m}$ for 2:1, $3.65 \pm 9.35 \mu\text{m}$ for 3:1, and only slightly increased to $5.00 \pm 15.49 \mu\text{m}$ for 4:1. This trend suggests that the DBM addition influenced particle agglomeration and dispersion within the composites (Table 4).

The elemental composition of each sample was analyzed using EDS, with the spectra shown in Figure 5 and quantitative data detailed in Table 5. The primary elements detected across all samples include carbon (C), oxygen (O), sodium (Na), magnesium (Mg), aluminum (Al), chlorine (Cl), and calcium (Ca).

Table 4. Particle size distribution of Ca(OH)_2 and DBM- Ca(OH)_2 composites of different ratios, measured by SEM.

Sample	Smallest Particle (μm)	Largest Particle (μm)	Average Particle Size (μm)	$\bar{x} \pm \text{SD}$
DBM *	-	-	-	-
Ca(OH)_2	0.01	350.68	6.34	6.34 ± 29.56
DBM- Ca(OH)_2 1:1	0.01	248.38	4.37	4.37 ± 13.42
DBM- Ca(OH)_2 2:1	0.01	149.67	4.50	4.50 ± 13.28
DBM- Ca(OH)_2 3:1	0.01	146.75	3.65	3.65 ± 9.35
DBM- Ca(OH)_2 4:1	0.01	197.28	5.00	5.00 ± 15.49

* Particle size measurements was not feasible for pure DBM. One sample from each group was used for this test.

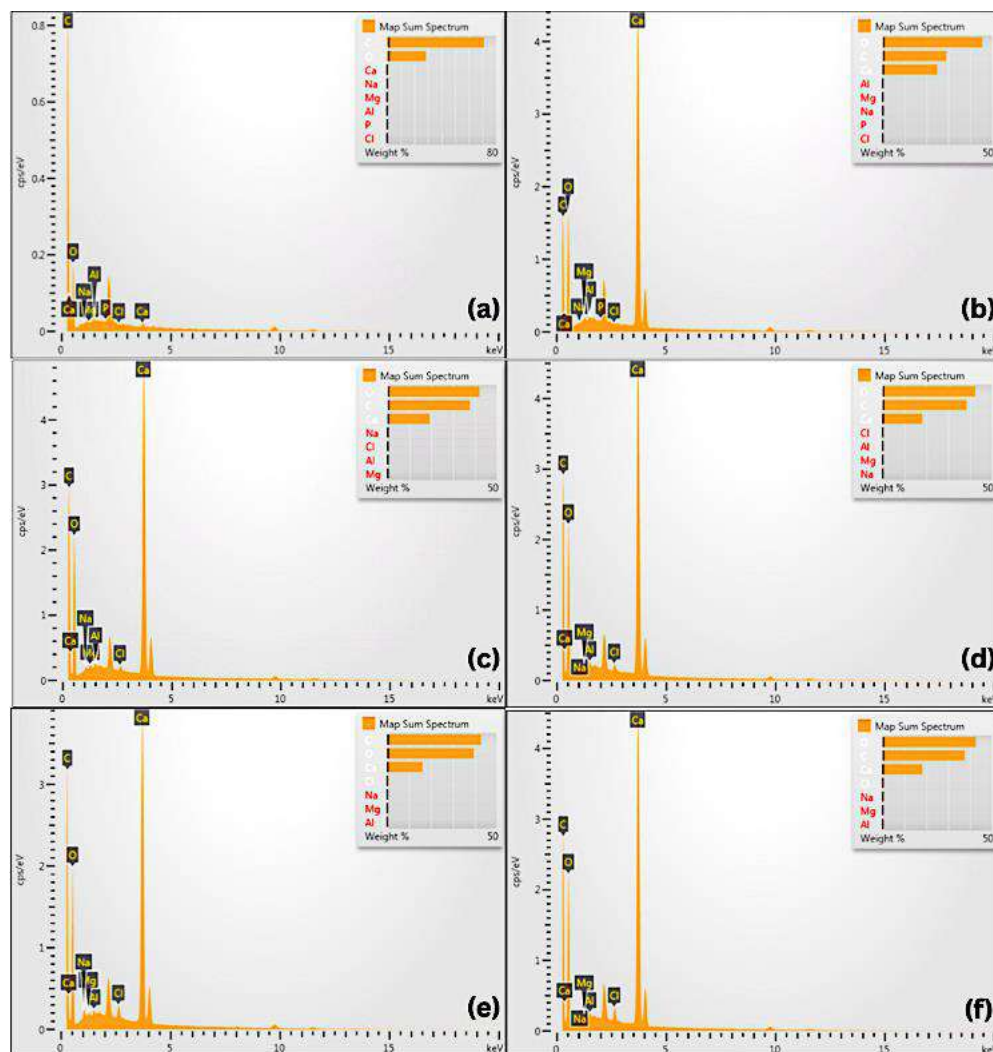


Figure 5. The Energy-Dispersive X-ray Spectroscopy (EDS) test results and the samples' composition: (a) DBM; (b) Ca(OH)_2 ; (c) DBM- Ca(OH)_2 1:1; (d) DBM- Ca(OH)_2 2:1; (e) DBM- Ca(OH)_2 3:1; (f) DBM- Ca(OH)_2 4:1.

In the pure DBM, carbon was the dominant element (71.14 wt%), reflecting the organic collagen in the matrix, with oxygen present at 28.51 wt%. In contrast, pure Ca(OH)_2 exhibited a higher oxygen content (45.55 wt%) and lower carbon content (29.04 wt%), consistent with its inorganic nature.

For DBM- Ca(OH)_2 composites, elemental compositions varied depending on their mixing ratio. Generally, their carbon and oxygen percentages shifted to intermediate values between those of pure DBM and Ca(OH)_2 , indicating the successful integration of

both components. Notably, the calcium content was maintained across the composites, supporting the presence of inorganic mineral phases critical for osteoconductivity, which contribute to the mechanical strength and stiffness of bone tissue. Phosphorus enhances the structural integrity and stability of bone. Carbon has been shown to promote the proliferation and differentiation of bone-forming cells within newly developing tissue. Meanwhile, oxygen facilitates the process of angiogenesis, which is essential for delivering nutrients and oxygen to the fracture site during the healing process.

These findings demonstrate the coexistence and homogeneous distribution of organic (DBM) and inorganic ($\text{Ca}(\text{OH})_2$) phases within the composites, which may enhance their biological and mechanical properties for bone regeneration applications.

Table 5. Elemental composition (weight percentage) of DBM, $\text{Ca}(\text{OH})_2$, and DBM- $\text{Ca}(\text{OH})_2$ composites, measured by EDS.

Element	DBM	$\text{Ca}(\text{OH})_2$	DBM- $\text{Ca}(\text{OH})_2$ 1:1	DBM- $\text{Ca}(\text{OH})_2$ 2:1	DBM- $\text{Ca}(\text{OH})_2$ 3:1	DBM- $\text{Ca}(\text{OH})_2$ 4:1
	Wt%	Wt%	Wt%	Wt%	Wt%	Wt%
C	71.14	29.04	37.7	38.47	42.89	37.60
O	28.51	45.55	42.13	42.35	39.66	42.70
Na	0	0	0.28	0.21	0.48	0.52
Mg	0	0.23	0.14	0.23	0.16	0.20
Al	0	0.24	0.2	0.23	0.15	0.19
Cl	0	0	0.25	0.31	0.53	0.6
Ca	0.35	24.94	19.3	18.2	16.12	18.2

One sample from each group was used for this test.

4. Discussion

This study explored the physicochemical and morphological properties of DBM- $\text{Ca}(\text{OH})_2$ composites with varying ratios to evaluate their potential as bone graft materials. Each analytical technique—XRD, AAS, FTIR, and SEM—provided valuable insights into how the combination of DBM- $\text{Ca}(\text{OH})_2$ influences structural, chemical, and surface characteristics that are critical for bone regeneration.

XRD analysis revealed important information about the crystallinity and phase composition of the composites. Pure $\text{Ca}(\text{OH})_2$ exhibited sharp and distinct diffraction peaks, which correspond to its well-ordered crystalline structure. These peaks serve as fingerprints confirming the presence of highly crystalline $\text{Ca}(\text{OH})_2$. When DBM was added to the composite in increasing proportions, the intensity of these crystalline peaks diminished noticeably. This decrease indicates a reduction in crystallinity due to the incorporation of DBM, which is predominantly amorphous and composed mainly of collagen and organic matrix components. The highest DBM ratio (4:1) showed the lowest peak intensity, suggesting that the amorphous phase of DBM increasingly disrupted the ordered crystalline lattice of calcium hydroxide.

The degree of crystallinity is a key factor influencing a material's behavior in biological environments. Lower crystallinity tends to enhance bioactivity by improving cell adhesion and accelerating degradation, which facilitates the natural bone remodeling process [31,32]. However, highly amorphous materials may lack sufficient mechanical strength to support this process. In this context, the 2:1 DBM- $\text{Ca}(\text{OH})_2$ composite exhibited moderate crystallinity, indicating a promising balance between maintaining enough structural integrity and providing an active surface favorable for osteoblast function [33]. This suggests that tuning the DBM-to- $\text{Ca}(\text{OH})_2$ ratio can modulate crystallinity and thus tailor the composite's performance to specific clinical needs.

Calcium ion release, as measured by AAS, is a crucial parameter because calcium ions regulate multiple cellular processes essential for bone formation, including osteoblast proliferation, differentiation, and mineralization [34,35]. The results showed that pure Ca(OH)_2 released the largest amount of calcium ions, reflecting its high solubility. Conversely, DBM released minimal calcium due to its largely organic, demineralized nature. Composite samples exhibited calcium release levels inversely proportional to their DBM content; as the amount of DBM present increased, calcium release decreased significantly [36–38].

Maintaining calcium ion release within an optimal physiological range is essential because while calcium is necessary for bone healing, excessive calcium concentrations can be cytotoxic to osteoblasts [39–41]. The ideal range for promoting osteogenic activity is generally between 60 and 90 mg/L. In this study, all composite formulations exceeded this range, but the DBM– Ca(OH)_2 composite (ratio 4:1) released the lowest calcium concentration, suggesting a more controlled release profile that might reduce potential cytotoxicity while still supporting bone regeneration. The DBM– Ca(OH)_2 composite created at a 2:1 ratio released higher levels of calcium, which could accelerate osteoblast activity and bone formation but might also increase the risk of cellular stress if concentrations become excessive. These findings highlight the importance of optimizing the composite's formulation to balance calcium availability with biological safety and efficacy.

The decreasing amount of calcium ion released with the increasing DBM content can be explained by the presence of collagen-rich, amorphous DBM, which reduces overall solubility and slows the diffusion of calcium ions from the composite. This slower and more sustained release may be advantageous for long-term bone healing, providing a steady supply of calcium ions that supports gradual mineralization without overwhelming the cellular environment [42]. In contrast, composites with lower DBM contents may degrade faster, releasing calcium ions rapidly but risking cytotoxicity and impaired osteoblast function [43]. Thus, both the 4:1 and 2:1 composites represent viable options, with the former offering safer, sustained release and the latter favoring faster bone regeneration.

Our FTIR analysis further clarified the chemical composition and molecular interactions within the composites. The DBM control exhibited characteristic absorption bands associated with amide groups (amide I, II, III, A, and B), confirming the presence of collagen, the primary organic component of bone matrix responsible for structural support and cell signaling [44,45]. In contrast, the Ca(OH)_2 (as control) displayed strong peaks related to hydroxyl and carbonate groups, consistent with its inorganic mineral composition and high alkalinity [46,47].

In the DBM– Ca(OH)_2 composites, the typical amide bands of collagen were diminished or absent, while phosphate and carboxylate ion peaks became more prominent [48,49]. This indicates that chemical changes occurred during composite preparation, likely due to hydrolysis reactions caused by the alkaline environment from the Ca(OH)_2 . These reactions may break the peptide bonds in collagen, generating carboxylate-containing groups and altering the organic matrix's structure [50–52]. The presence of phosphate bands suggests that residual mineral components remain within the composite despite the demineralization process. These phosphate groups could enhance osteoconductivity by supporting mineral deposition during bone formation. Understanding these molecular-level changes is vital because they influence both the mechanical properties and the biological responses elicited by the composite graft.

SEM provided critical morphological data, revealing how surface texture, particle size, and shape affect the composite's interaction with cells and its overall bioactivity [53–55]. Rough surface structures were observed, particularly in the DBM– Ca(OH)_2 composite (ratio 4:1), consistent with previous studies demonstrating that roughness enhances protein

adsorption and promotes osteoblast attachment, proliferation, and differentiation [56,57]. These factors are essential for effective osseointegration and bone regeneration.

Particle size also influences the biological response. Although the literature often cites particles of around 100 μm as optimal for osteoblast activation [28], the microparticle size observed in the composites ($\sim 5 \mu\text{m}$) falls within a size range shown to positively affect bone growth factors and increase the surface area available for cellular interactions. Smaller particles may also improve resorbability, allowing the graft to be gradually replaced by new bone tissue.

Regarding particle shape, Ca(OH)_2 typically appears as small granular or blocky particles, while DBM forms flake-like fragments [58,59]. In the DBM– Ca(OH)_2 composite, particle morphology became more uniform and denser, especially at the 4:1 ratio. This denser particle arrangement likely facilitates mechanical interlocking and enhances cellular adhesion, both of which are beneficial for osteogenesis and graft stability [60,61]. Together, these morphological features reinforce the composite's suitability as a scaffold for bone healing.

In summary, the results demonstrate that increasing the amount of DBM in the DBM– Ca(OH)_2 composite influences its crystallinity, calcium release profile, chemical composition, and surface morphology, all of which affect its biological performance. The 4:1 composite exhibits a lower crystallinity, controlled calcium ion release, chemically modified organic components, and an optimal surface morphology that collectively support sustained bone regeneration with potentially reduced cytotoxicity. The 2:1 composite maintains moderate crystallinity and releases higher concentrations of calcium, offering a balance between mechanical support and accelerated bioactivity.

Both composite formulations hold promise as bone graft materials. However, further biological studies, including cell cultures and in vivo bone regeneration models, are necessary to validate their osteogenic potential and optimize their ratios for specific clinical applications. In addition, further in vitro studies are recommended to assess the cytocompatibility of the ions released from the composites, which is critical for ensuring their safety and effectiveness in biological environments. This multiparametric characterization provides a solid foundation for designing bone graft substitutes with properties that are tailored to meet diverse therapeutic needs. Another limitation of this study is that the particle size, crystallinity, and elemental analyses were each conducted on a single sample per formulation. As such, statistical comparisons could not be performed; further replicates are recommended in future studies to ensure reproducibility and assess variability.

5. Conclusions

This study investigated the physicochemical and compositional characteristics of DBM– Ca(OH)_2 composites with varying ratios to identify a formulation suitable for bone regeneration. Increasing the DBM content in the composite led to a reduction in crystallinity and calcium ion release, along with a modulation of particle size distribution. These changes reflect a shift toward a more bioresorbable and biologically responsive material.

Among the tested formulations, the 2:1 DBM– Ca(OH)_2 ratio demonstrated an optimal balance. It maintained sufficient calcium availability to support osteogenic activity, exhibited a moderately reduced crystallinity conducive to biodegradation, and presented a favorable average particle size that may enhance cellular attachment and proliferation. The composite also retained the essential organic and inorganic functional groups from both components, suggesting successful integration and the potential for mineralized tissue formation. Overall, the DBM– Ca(OH)_2 composite at a 2:1 ratio is a promising candidate for bone graft applications, offering a combination of structural support and biological functionality.

6. Patents

The work reported in this manuscript resulted in a patent granted by the Directorate General of Intellectual Property (DJKI) under the number EC00202517207.

Author Contributions: Conceptualization, O., F.L.K. and O.N.K.; methodology, O., F.L.K. and O.N.K.; software, F.A.L.; validation, O., F.L.K. and O.N.K.; formal analysis, F.A.L.; investigation, F.A.L.; resources, O., F.L.K. and O.N.K.; data curation, F.A.L.; writing—original draft preparation, F.A.L.; writing—review and editing, O., F.L.K., O.N.K. and M.D.C.S.; visualization, F.A.L. and M.D.C.S.; supervision, O., F.L.K. and O.N.K.; project administration, O., F.L.K. and O.N.K.; funding acquisition, O., F.L.K. and O.N.K. All authors have read and agreed to the published version of the manuscript.

Funding: This research was fully funded by Universitas Trisakti under contract number 360/A.1/LPPM-P/USAKTI/X/2024.

Institutional Review Board Statement: This study was approved by the Ethics Committee of Universitas Trisakti (783/S1/KEPK/FGK/6/2024, 14 June 2024, and 839/S1/KEPK/FGK/7/2024, 5 July 2024).

Data Availability Statement: The raw data supporting the conclusions of this article will be made available by the authors on request.

Conflicts of Interest: The authors declare no conflicts of interest.

References

1. Nibali, L.; Sultan, D.; Arena, C.; Pelekos, G.; Lin, G.; Tonetti, M. Periodontal infrabony defects: Systematic review of healing by defect morphology following regenerative surgery. *J. Clin. Periodontol.* **2021**, *48*, 100–113. [[CrossRef](#)] [[PubMed](#)]
2. Tsuchida, S.; Nakayama, T. Recent clinical treatment and basic research on the alveolar bone. *Biomedicines* **2023**, *11*, 843. [[CrossRef](#)] [[PubMed](#)]
3. Boehm, T.K.; Clara, S.K. *An Overview of Periodontal Surgical Procedures*; StatPearls Publishing: Treasure Island, FL, USA, 2024.
4. Ciszynski, M.; Dominiak, S.; Dominiak, M.; Gedrange, T.; Hadzik, J. Allogenic bone graft in dentistry: A review of current trends and developments. *Int. J. Mol. Sci.* **2023**, *24*, 16598. [[CrossRef](#)]
5. Zhang, X.; Li, Q.; Wang, Z.; Zhou, W.; Zhang, L.; Liu, Y.; Xu, Z.; Li, Z.; Zhu, C.; Zhang, X. Bone regeneration materials and their application over 20 years: A bibliometric study and systematic review. *Front. Bioeng. Biotechnol.* **2022**, *10*, 921092. [[CrossRef](#)]
6. Wibowo, A.R.; Octarina, O.; Munadzirah, E.; Handharyani, E. The effect of application bovine amniotic membrane on osteoblasts, osteocytes, and collagen. *Padjajaran J. Dent.* **2023**, *35*, 163–169. [[CrossRef](#)]
7. Veremeev, A.; Bolgarin, R.; Nesterenko, V.; Andreev-Andrievskiy, A.; Kutikhin, A. Native bovine hydroxyapatite powder, demineralised bone matrix powder, and purified bone collagen membranes are efficient in repair of critical-sized rat calvarial defects. *Materials* **2020**, *13*, 3393. [[CrossRef](#)]
8. Zhang, H.; Yang, L.; Yang, X.-G.; Wang, F.; Feng, J.; Hua, K.; Li, Q.; Hu, Y. Demineralized bone matrix carriers and their clinical applications: An overview. *Orthop. Surg.* **2019**, *11*, 725–737. [[CrossRef](#)] [[PubMed](#)]
9. Chen, I.-C.; Su, C.-Y.; Lai, C.-C.; Tsou, Y.-S.; Zheng, Y.; Fang, H.-W. Preparation and characterization of moldable demineralized bone matrix/calcium sulfate composite bone graft materials. *J. Funct. Biomater.* **2021**, *12*, 56. [[CrossRef](#)] [[PubMed](#)]
10. Wen, B.; Freilich, M.; Kuhn, L. Bone Tissue Engineering Around Dental Implants. *Stem Cell Biol. Tissue Eng. Dent. Sci.* **2015**, *55*, 749–764.
11. Cho, H.; Bucciarelli, A.; Kim, W.; Jeong, Y. Natural Sources and Applications of Demineralized Bone Matrix in the Field of Bone and Cartilage Tissue Engineering. *Adv. Exp. Med. Biol.* **2020**, *1249*, 3–14.
12. Sawkins, M.; Bowen, W.; Dhadha, P.; Markides, H.; Sidney, L.; Taylor, A.; Rose, F.; Badylak, S.; Shakesheff, K.; White, L. Hydrogels derived from demineralized and decellularized bone extracellular matrix. *Acta Biomater.* **2013**, *9*, 7865–7873. [[CrossRef](#)] [[PubMed](#)]
13. Verboket, R.D.; Irrle, T.; Busche, Y.; Schaible, A.; Schröder, K.; Brune, J.C.; Marzi, I.; Nau, C.; Henrich, D. Fibrous demineralized bone matrix (DBM) improves bone marrow mononuclear cell (BMC)-supported bone healing in large femoral bone defects in rats. *Cells* **2021**, *10*, 1249. [[CrossRef](#)] [[PubMed](#)]
14. Khosropanah, H.; Lashkarizadeh, N.; Ayatollahi, M.; Kaviani, M.; Mostafavipour, Z. The impact of calcium hydroxide on the osteoinductive capacity of demineralized freeze-dried bone allograft: An in-vitro study. *J. Dent. Shiraz. Univ. Med. Sci.* **2018**, *19*, 19–27.
15. Mahajan, A.; Kedige, S. Periodontal bone regeneration in intrabony defects using osteoconductive bone graft versus combination of osteoconductive and osteostimulative bone graft: A comparative study. *J. Dent. Res.* **2015**, *12*, 25–30. [[CrossRef](#)]

16. Khorshidi, H.; Raoofi, S.; Sabagh, S.; Behboud, Z.; Mozafari, G.; Ashraf, M. Effect of combined calcium hydroxide and accelerated portland cement on bone formation and soft tissue healing in dog bone lesions. *J. Dent. Biomater.* **2015**, *2*, 97–102.
17. Dhruvakumar, D.; Gupta, C. Role of combination therapy/composite graft in periodontal regeneration: A mini review. *Tanta Dent. J.* **2017**, *14*, 169. [[CrossRef](#)]
18. Barus, L.; Septianingtyas, V.; Febriadi, P.B.; Hendra, I.M.; Annis, A.F.; Satria, R.M.H.; Wibisono, N.I.; Pratiwi, E.S.; Rasyida, A.Z.; Mulyawan, I.; et al. Demineralized Freeze-Dried Bovine Bone Xenograft Granules as Alveolar Bone Substitutes: A Profile Study. 2021. Available online: <http://www.jidmr.com> (accessed on 8 June 2025).
19. Coathup, M.; Champion, C.; Blunn, G. A carboxymethyl cellulose bone graft carrier delays early bone healing in an ovine model. *J. Biomed. Mater. Res.-Part B Appl. Biomater.* **2020**, *108*, 612–618. [[CrossRef](#)]
20. Chauhan, N.; Lakhkar, N.; Chaudhari, A. Development and physicochemical characterization of novel porous phosphate glass bone graft substitute and in vitro comparison with xenograft. *J. Mater. Sci. Mater. Med.* **2021**, *32*, 60. [[CrossRef](#)]
21. Kurniawan, F.L.; Tjandrawinata, R.; Marpaung, C.; Pratiwi, D.; Komariah, K. The effect of horn beetle nanochitosan (*Xylotrupes gideon*) addition on the hardness of glass-ionomer cement. *J. Indones. Dent. Assoc.* **2022**, *5*, 27–31. [[CrossRef](#)]
22. Livia, F.; Tjandrawinata, R.; Marpaung, C.D.; Pratiwi, D.; Komariah, K. The effect of horn beetle nano chitosan (*Xylotrupes gideon*) on the surface roughness of glass-ionomer cement. *Mater. Sci. Forum.* **2022**, *1069*, 161–166. [[CrossRef](#)]
23. Ali, A.; Chiang, Y.W.; Santos, R.M. X-ray diffraction techniques for mineral characterization: A review for engineers of the fundamentals, applications, and research firections. *Minerals* **2022**, *12*, 205. [[CrossRef](#)]
24. Khan, H.; Yerramilli, A.S.; D'Oliveira, A.; Alford, T.L.; Boffito, D.C.; Patience, G.S. Experimental methods in chemical engineering: X-ray diffraction spectroscopy—XRD. *Can. J. Chem. Eng.* **2020**, *98*, 1255–1266. [[CrossRef](#)]
25. Filio, P.; Octarina, F.; Komariah, F. Characterization of fabricated bovine hydroxyapatite crystal as socket preservation material: An SEM-EDX and x-ray diffraction study. *World J. Dent.* **2022**, *13* (Suppl. S2), S175–S181. [[CrossRef](#)]
26. Filho, H.J.I.; Salazar, R.F.S.; Capri, M.R.; Neto, A.C.; Alcantara, M.A.K.; Peixoto, A.L.C. State-of-the-art and trends in atomic absorption spectrometry. In *Atomic Absorption Spectroscopy*; InTech: Houston, TX, USA, 2012; pp. 13–36.
27. Berna, F. *Encyclopedia of Geoarchaeology*; Springer: Dordrecht, The Netherlands, 2017.
28. Nam, J.-W.; Kim, M.-Y.; Han, S.-J. Cranial Bone Regeneration According to Different Particle Sizes and Densities of Demineralized Dentin Matrix in The Rabbit Model. *Maxillofac. Plast. Reconstr. Surg.* **2016**, *38*, 27. [[CrossRef](#)]
29. Charlena, C.; Maddu, A.; Hidayat, T. Synthesis and Characterization of hydroxyapatite from green mussel shell with sol-gel method. *J. Kim. Val.* **2022**, *8*, 269–279. [[CrossRef](#)]
30. Widjonarko, N.E. Introduction to advanced x-ray diffraction techniques for polymeric thin films. *Coatings* **2016**, *6*, 54. [[CrossRef](#)]
31. Dozza, B.; Lesci, I.G.; Duchi, S.; Della Bella, E.; Martini, L.; Salamanna, F.; Falconi, M.; Cinotti, S.; Fini, M.; Lucarelli, E.; et al. When size matters: Differences in demineralized bone matrix particles affect collagen structure, mesenchymal stem cell behaviour, and osteogenic potential. *J. Biomed. Mater. Res.* **2017**, *105*, 1019–1033. [[CrossRef](#)]
32. Nicoletti, A.; Torricelli, P.; Bigi, A.; Fornasari, P.; Fini, M.; Moroni, L. Incorporation of nanostructured hydroxyapatite and poly(*N*-isopropylacrylamide) in demineralized bone matrix enhances osteoblast and human mesenchymal stem cell activity. *Biointerphases* **2015**, *10*, 041001. [[CrossRef](#)]
33. Chacón, V.P.G.; Habibovic, P. Deconvoluting the bioactivity of calcium phosphate-based bone graft substitutes: Strategies to understand the role of individual material properties. *Adv. Healthc. Mater.* **2017**, *6*, 1601478. [[CrossRef](#)]
34. Mohammadi, M.; Shaegh, S.A.M.; Alibolandi, M.; Ebrahimzadeh, M.H.; Tamayol, A.; Jaafari, M.R.; Ramezani, M. Micro and nanotechnologies for bone regeneration: Recent advances and emerging designs. *J. Control. Release* **2018**, *274*, 35–55. [[CrossRef](#)]
35. Manalu, J.L.; Soegijono, B.; Indrani, D.J. Characterization of hydroxyapatite derived from bovine bone. *Asian J. Appl. Sci.* **2015**, *3*, 758–765.
36. Ovrebø, O.; Orlando, L.; Rubenis, K.; Ciriello, L.; Ma, Q.; Giorgi, Z.; Tognoni, S.; Loca, D.; Villa, T.; Nogueira, L.P.; et al. The role of collagen and crystallinity in the physicochemical properties of naturally derived bone grafts. *Regen. Biomater.* **2024**, *11*, rbae093. [[CrossRef](#)] [[PubMed](#)]
37. Hong, K. Analysis of crystal structure of bone graft material using analyses of x-Ray diffraction and scanning electron microscope image. *Int. J. Clin. Prev. Dent.* **2019**, *15*, 215–219. [[CrossRef](#)]
38. Park, M.; Mah, Y.J.; Kim, D.H.; Kim, E.S.; Park, E.J. Demineralized deciduous tooth as a source of bone graft material: Its biological and physicochemical characteristics. *Oral Surg. Oral Med. Oral Pathol. Oral Radiol.* **2015**, *120*, 307–314. [[CrossRef](#)]
39. Haugen, H.J.; Lyngstadaas, S.P.; Rossi, F.; Perale, G. Bone grafts: Which is the ideal biomaterial. *J. Clin. Periodontol.* **2019**, *46* (Suppl. S21), 92–102. [[CrossRef](#)]
40. Montazerian, M.; Shearer, A.; Mauro, J.C. Perspectives on the impact of crystallization in bioactive glasses and glass-ceramics. *Int. J. Ceram. Eng. Sci.* **2023**, *6*, e10194. [[CrossRef](#)]
41. Kuzmenka, D.; Sewohl, C.; König, A.; Flath, T.; Hahnel, S.; Schulze, F.P.; Hacker, M.C.; Schulz-Siegmund, M. Sustained calcium(II)-release to impart bioactivity in hybrid glass scaffolds for bone tissue engineering. *Pharmaceutics* **2020**, *12*, 1192. [[CrossRef](#)]

42. Berberi, A.; Samarani, A.; Nader, N.; Noujeim, Z.; Dagher, M.; Kanj, W.; Mearawi, R.; Saleme, Z.; Badran, B. Physicochemical characteristics of bone substitutes used in oral surgery in comparison to autogenous bone. *BioMed Res. Int.* **2014**, *2014*, 320790. [[CrossRef](#)]
43. Sunarso; Rahmawati, D.; Irawan, B.; Pangesty, A.I. A novel method to fabricate monetite granules for bone graft applications. *Dent. Mater. J.* **2024**, *43*, 67–73. [[CrossRef](#)]
44. Roldan, L.; Isaza, C.; Ospina, J.; Montoya, C.; Domínguez, J.; Orrego, S.; Correa, S. A Comparative Study of HA/DBM Compounds Derived from Bovine and Porcine for Bone Regeneration. *J. Funct. Biomater.* **2023**, *14*, 439. [[CrossRef](#)]
45. Suptijah, P.; Indriani, D.; Wardoyo, S.E. Isolasi dan karakterisasi kolagen dari kulit ikan patin (*Pangasius* sp.). *J. Sains Nat.* **2018**, *8*, 8–23. [[CrossRef](#)]
46. Kiefer, J.; Stärk, A.; Kiefer, A.; Glade, H. Infrared Spectroscopic Analysis of the Inorganic Deposits from Water in Domestic and Technical Heat Exchangers. *Energies* **2018**, *11*, 798. [[CrossRef](#)]
47. Riaz, T.; Zeeshan, R.; Zarif, F.; Ilyas, K.; Muhammad, N.; Safi, S.Z.; Rahim, A.; Rizvi, S.A.A.; Rehman, I.U. FTIR analysis of natural and synthetic collagen. *Appl. Spectrosc. Rev.* **2018**, *53*, 703–746. [[CrossRef](#)]
48. Idiawati, N.; Novita, I.; Nurdiansyah, S.I.; Minsas, S.; Siregar, S. Identifikasi kolagen dari cangkang bulu babi (*Diadema setosum*) asal perairan Pulau Lemukutan. *Marinade* **2022**, *5*, 136–141. [[CrossRef](#)]
49. Sizeland, K.H.; Hofman, K.A.; Hallett, I.C.; Martin, D.E.; Potgieter, J.; Kirby, N.M.; Hawley, A.; Mudie, S.T.; Ryan, T.M.; Haverkamp, R.G.; et al. Nanostructure of electrospun collagen: Do electrospun collagen fibers form native structures? *Materialia* **2018**, *3*, 90–96. [[CrossRef](#)]
50. Hossain, M.S.; Ahmed, S. FTIR spectrum analysis to predict the crystalline and amorphous phases of hydroxyapatite: A comparison of vibrational motion to reflection. *RSC Adv.* **2023**, *13*, 14625–14630. [[CrossRef](#)]
51. Nandiyanto, A.B.D.; Oktiani, R.; Ragadhita, R. How to Read and Interpret FTIR Spectroscopy of Organic Material. *Indones. J. Sci. Technol.* **2019**, *4*, 97. [[CrossRef](#)]
52. Febri, W.; Astuti, E.; Trisnawati, P. Uji Hidrolisis Parasetamol dalam Larutan pH 2,0; 5,0; dan 7,0 Pada Suhu 37 °C. Bachelor's Thesis, Program Studi Farmasi, Fakultas Sains dan Teknologi, Universitas Peradaban, 2022. Available online: <http://repository.peradaban.ac.id/id/eprint/1076> (accessed on 8 June 2025).
53. Bariyah, N.; Pascawinata, A.; Firdaus, F. Gambaran Karakteristik Scaffold Hidroksiapatit Gigi Manusia Dengan Metode Planetary Ball Mill Menggunakan Uji Scanning Electron Microscope (Sem). *B-Dent. Kedokt. Gigi Univ. Baiturrahmah* **2016**, *3*, 131–138. [[CrossRef](#)]
54. Munadzirroh, E.; Razak, F.A.; Abbas, B.; Soekartono, H.; Agustantina, T.H.; Surboyo, M.D. Characterization of bovine sponge amnion (BSA) by a novel process for dental treatment. *J. Int. Dent. Med. Res.* **2022**, *15*, 479–484.
55. O'Connor, D.; Sexton, B.; Smart, R. *Surface Analysis Methods in Materials Science*; Springer Series in Surface Sciences; Springer Nature: Dordrecht, The Netherlands, 2013.
56. Dewi, M.; Peornomo, H. The Effect of Zirconia Material for Dental Implant to Osseointegrated Process. *SONDE (Sound Dent.)* **2020**, *5*, 39–53. [[CrossRef](#)]
57. Le Guéhennec, L.; Soueidan, A.; Layrolle, P.; Amouriq, Y. Surface treatments of titanium dental implants for rapid osseointegration. *Dent. Mater.* **2007**, *23*, 844–854. [[CrossRef](#)] [[PubMed](#)]
58. Engbrecht, D.C.; Hirschfeld, D. Thermal analysis of calcium sulfate dihydrate sources used to manufacture gypsum wallboard. *Thermochim. Acta* **2016**, *639*, 173–185. [[CrossRef](#)]
59. Grawish, M.E. Demineralized dentin matrix for dental and alveolar bone tissues regeneration: An innovative scope review. *Tissue Eng. Regen. Med.* **2022**, *19*, 687–701. [[CrossRef](#)] [[PubMed](#)]
60. Li, Q. Demineralized bone matrix-based microcarrier scaffold favors vascularized large bone regeneration in vivo in a rat model. *J. Biomater. Appl.* **2018**, *33*, 182–195. [[CrossRef](#)]
61. Leni, A.; Hariyani, N.A. Hidroksiapatit sebagai salah satu bahan yang paling umum digunakan pada cangkok tulang. *J. Kedokt. Gigi Univ. Baiturrahmah* **2021**, *8*, 172–178. [[CrossRef](#)]

Disclaimer/Publisher's Note: The statements, opinions and data contained in all publications are solely those of the individual author(s) and contributor(s) and not of MDPI and/or the editor(s). MDPI and/or the editor(s) disclaim responsibility for any injury to people or property resulting from any ideas, methods, instructions or products referred to in the content.

Physicochemical Properties of Demineralized Bone Matrix and Calcium Hydroxide Composites Used as Bone Graft Material

by Octarina FKG

Submission date: 21-Jul-2025 11:45AM (UTC+0700)

Submission ID: 2587380493

File name: crystals-15-00564.pdf (1.98M)

Word count: 7860

Character count: 42672

Article

Physicochemical Properties of Demineralized Bone Matrix and Calcium Hydroxide Composites Used as Bone Graft Material

Octarina ¹, Florencia Livia Kurniawan ^{1,*}, Firda Amalia Larosa ¹, Olivia Nauli Komala ² and Meircurius Dwi Condro Surboyo ³

¹ Department of Dental Material, Faculty of Dentistry Universitas Trisakti, Jakarta 11440, Indonesia; octarina@trisakti.ac.id (O.); famalia02@gmail.com (F.A.L.)

² Department of Periodontics, Faculty of Dentistry Universitas Trisakti, Jakarta 11440, Indonesia; olivia.nauli@trisakti.ac.id

³ Department of Oral Medicine, Faculty of Dental Medicine, Universitas Airlangga, Surabaya 60132, Indonesia; meircurius-2015@fkg.unair.ac.id

* Correspondence: florencia@trisakti.ac.id

Abstract: Vertical bone defects can result in alveolar bone resorption, which may be addressed using composite grafts. A combination of demineralized bone matrix (DBM) and calcium hydroxide (Ca(OH)₂) has potential as a bone substitute due to its biological and structural properties. This study aimed to identify the optimal DBM–Ca(OH)₂ ratio by evaluating their physicochemical properties relevant to bone regeneration. DBM gel and Ca(OH)₂ powder were combined at ratios of 1:1, 2:1, 3:1, and 4:1. The mixtures were freeze-dried, ground, and sieved to create granules. The composites were analyzed in terms of their structural and chemical characteristics, including crystallinity, calcium ion release, functional group composition, particle size, surface morphology, and elemental distribution. Increasing the proportion of DBM reduced crystallinity and calcium ion release while influencing particle size. Among all groups, the 2:1 composite demonstrated the most balanced properties: moderate crystallinity, relatively high calcium release, and favorable particle size. Chemical analyses confirmed the presence and interaction of both organic and inorganic components, while elemental mapping showed a uniform distribution of the key elements essential for bone formation. The DBM–Ca(OH)₂ composite at a 2:1 ratio has the most promising physicochemical profile, making it a strong candidate for bone graft applications. However, a limitation of this study is the absence of biological testing. Future research should investigate the in vitro and in vivo performance of this composite in bone regeneration.

Keywords: bone graft; demineralized bone matrix; calcium hydroxide; crystallinity; solubility; functional groups; surface morphology



check for updates

Academic Editor: Michele Iafisco

Received: 16 April 2025

Revised: 3 June 2025

Accepted: 9 June 2025

Published: 15 June 2025

Citation: Octarina, Kurniawan, F.L.; Larosa, F.A.; Komala, O.N.; Surboyo, M.D.C. Physicochemical Properties of Demineralized Bone Matrix and Calcium Hydroxide Composites Used as Bone Graft Material. *Crystals* **2025**, *15*, 564. <https://doi.org/10.3390/cryst15060564>

Copyright: © 2025 by the authors. Licensee MDPI, Basel, Switzerland. This article is an open access article distributed under the terms and conditions of the Creative Commons Attribution (CC BY) license (<https://creativecommons.org/licenses/by/4.0/>).

1. Introduction

Vertical bone defects, characterized by bone loss extending below the alveolar crest, can lead to significant alveolar bone resorption, often requiring a periodontal surgical intervention to restore bone integrity [1,2]. Periodontal flap surgery aims to remove damaged tissue and promote healing and is often supported by bone grafts that serve as scaffolds to stimulate new bone growth and repair defects [3,4]. Optimizing these graft materials is crucial to improving outcomes in periodontal therapy, especially for complex bone loss, where it may help avoid dental procedures such as denture placement [5,6].

Demineralized bone matrix (DBM), derived from bovine bone, undergoes demineralization to remove organic components and retain inorganic components—especially

hydroxyapatite ($\text{Ca}_{10}(\text{PO}_4)_6(\text{OH})_2$)—reducing its crystallinity and mimicking the composition of human bone. DBM contains collagen, non-collagenous proteins, and growth factors like bone morphogenetic proteins (BMPs) and transforming growth factor-beta (TGF- β) [7,8], which contribute to its osteoinductive properties by promoting osteogenic differentiation and bone formation [9,10]. Its collagen matrix provides an osteoconductive scaffold that supports cell attachment and proliferation during bone healing [11,12]. However, demineralization lowers its calcium content, making supplementation necessary to enhance DBM's bone-forming potential [13].

Calcium hydroxide ($\text{Ca}(\text{OH})_2$) supplies osteoinductive calcium ions, encourages hard tissue formation, possesses antibacterial properties due to its alkalinity, and stimulates angiogenesis through growth factor release [14–16]. Combining DBM with $\text{Ca}(\text{OH})_2$ has been shown to improve osteoinductive activity, supporting osteoblast proliferation and mineralization [14]. Composite grafts containing these materials can harness both osteoconductive and osteoinductive effects, improving bone regeneration [17]. Granular DBM- $\text{Ca}(\text{OH})_2$ composites at ratios of 1:1, 2:1, 3:1, and 4:1 were developed, offering favorable structure, morphology, and clinical handling [18,19].

Physicochemical characteristics, such as crystallinity, calcium content, chemical bonding, and surface morphology, directly influence graft performance and bone regeneration potential [20–22]. Although previous studies have explored the individual use and combined application of DBM and $\text{Ca}(\text{OH})_2$, comprehensive data on the composite's physicochemical properties, especially in granular form, remain limited. There is a lack of detailed characterization used to determine how varying DBM- $\text{Ca}(\text{OH})_2$ ratios affect key parameters essential for bone graft efficacy. To address this gap, the present study uses X-ray diffraction (XRD) to evaluate the composite's crystallinity and phase composition [23–25]; Atomic Absorption Spectroscopy (AAS) to quantify its calcium ion concentration and solubility [26]; Fourier Transform Infrared Spectroscopy (FTIR) to identify functional groups and chemical interactions [27]; and Scanning Electron Microscopy with Energy-Dispersive X-ray Spectroscopy (SEM-EDS) to analyze its surface morphology, particle size, and elemental distribution [28]. This approach aims to identify the optimal DBM- $\text{Ca}(\text{OH})_2$ ratio with physicochemical properties suitable for further biological evaluation as a bone graft material.

Understanding these properties is essential as crystallinity influences biodegradability and osteoblast adhesion, solubility relates to material degradation and bone remodeling balance, and surface morphology and elemental composition impact cell attachment and osteoconductivity [29]. Although both DBM and $\text{Ca}(\text{OH})_2$ possess osteoinductive potential, the optimal physicochemical balance for bone regeneration has not been clearly established. It is hypothesized that increasing the proportion of DBM in the DBM- $\text{Ca}(\text{OH})_2$ composite will result in a lower overall crystallinity due to the amorphous nature of the demineralized matrix, which lacks ordered mineral phases. Additionally, despite undergoing demineralization, the DBM retains residual calcium and may facilitate greater calcium ion release through its organic matrix, potentially leading to higher detectable calcium concentrations than $\text{Ca}(\text{OH})_2$ alone. This unique combination may enhance ion availability and elemental distribution, improving the material's potential for bone grafting applications. Therefore, it is hypothesized that a DBM-rich composite will demonstrate a favorable crystallinity, calcium ion availability, and surface morphology, making it a promising candidate for further bone regeneration studies. This study aims to determine the optimal ratio of DBM- $\text{Ca}(\text{OH})_2$ (1:1, 2:1, 3:1, 4:1) in composite grafts by analyzing various physicochemical parameters, like crystallinity, solubility, functional groups, and surface morphology, in order to evaluate their potential suitability as bone graft materials.

2. Materials and Methods

2.1. Fabrication of DBM-Ca(OH)₂

Cortical bovine bone was obtained from a licensed slaughterhouse in Surabaya, East Java. The bone was cut into small sections and thoroughly cleaned using hydrogen peroxide (H₂O₂) to remove surface contaminants. To defat the bone, samples were immersed in an ultrasonic shaker kept at 60 °C until they appeared white and free of fatty tissue. The defatted bone was rinsed 3–4 times with distilled water to remove any residual peroxide and reduce toxicity.

The cleaned bone was demineralized by immersion in 1% hydrochloric acid (HCl), which removed the inorganic material while preserving the organic matrix. Following demineralization, the samples were rinsed 3–4 times with distilled water to eliminate residual acid. The demineralized bone was then mixed with 0.9% sodium chloride (NaCl) solution in a 1:1 ratio and homogenized using a blender to produce DBM gel.

Composite preparation was performed at the Tissue Bank, Dr. Soetomo Hospital, Surabaya, East Java. DBM gel and calcium hydroxide (Ca(OH)₂) powder (Merck, Darmstadt, Germany) were combined at four different weight ratios: 1:1, 2:1, 3:1, and 4:1. Each mixture was homogenized using a magnetic stirrer until a uniform consistency was achieved.

The homogenized mixtures were poured into 10 cm diameter Petri dishes and frozen at −80 °C for 24 h. Freeze-drying was conducted for 48 h at −100 °C to obtain a dry composite. The dried samples were then ground using a bone miller and sieved through a mesh (>710 µm) to obtain uniform granules (Figure 1).



Figure 1. DBM-Ca(OH)₂ prepared for four different weight ratios: 1:1, 2:1, 3:1, and 4:1.

2.2. X-Ray Diffraction (XRD)

The sample, initially in granule form, was ground into a fine powder to ensure homogeneity and improve its diffraction quality. An total of 1 g of the powdered sample was prepared for each experimental group. X-ray diffraction (XRD) analysis was performed using CuK α radiation ($\lambda = 1.5406 \text{ \AA}$) with a scan range of 10° to 90° (2 θ) and a step size of 0.01°. The X-ray diffraction (XRD) peaks obtained from the analysis were compared with standard reference patterns of known crystal structures to identify the crystalline phases present in the sample [30]. This phase identification was carried out using “Match!” software 3.15 version, which utilizes crystallographic databases such as ICDD. Furthermore, the diffraction peak’s characteristics—including its intensity, position, and full width at half maximum (FWHM)—were used to evaluate the degree of crystallinity and estimate the crystallite size. The degree of crystallinity was quantified using “Origin 2024 (10.1)

version" software through peak deconvolution and area integration methods, providing insights into the structural ordering of the material.

2.3. Atomic Absorption Spectroscopy (AAS)

To assess their calcium ion release, 25 mg of each granulated DBM-Ca(OH)₂ sample was immersed in 25 mL of Tris-HCl buffer (pH 7.4) to simulate physiological conditions. The samples were incubated at 37 °C for 7 days. Post-incubation, the solutions were filtered using Whatman filter paper to remove particulates. The calcium ion concentration of the filtrate was then quantified using a Thermo Scientific iCE 3000 Series Atomic Absorption Spectrometer (AAS) Waltham City, Massachusetts, United States.

The AAS system operated with acetylene gas and an airflow adjusted to the recommended pressure settings. The instrument's flame and hollow cathode lamp, which are specifically used for calcium, were activated, and the sample solutions were aspirated into the spray chamber. Measurements were taken at a wavelength of 422.7 nm, and calcium concentrations were recorded in mg/L.

2.4. Fourier Transform Infrared (FTIR) Spectroscopy

The sample, initially in granule form, was subjected to functional group analysis using an IR Prestige-21 FTIR spectrometer (Shimadzu, Japan). To enhance homogeneity, the granules were finely ground and thoroughly mixed with potassium bromide (KBr) and then pressed into transparent pellets to optimize their spectral resolution.

Measurements were performed using the Diffuse Reflectance-Fourier Transform Infrared Spectroscopy (DRS-FTIR) technique over a spectral range of 400–4000 cm⁻¹. The spectrometer operated at a resolution of 2.0 cm⁻¹, and each spectrum was averaged from 20 scans. Spectra were recorded as percent transmittance and analyzed to identify functional groups based on their characteristic absorption bands.

FTIR spectral data were compared with reference databases to determine functional group identities. Further analysis and visualization of absorption peaks were conducted using Origin software to support their interpretation and facilitate comparison.

2.5. Scanning Electron Microscope (SEM)—Energy-Dispersive X-Ray Spectroscopy (EDS)

Prior to imaging, the sample was mounted on a specimen holder and sputter-coated with a thin layer of gold-palladium to enhance its electrical conductivity and reduce charging effects. SEM imaging was performed under high-vacuum conditions using an accelerating voltage of 20 kV, a working distance of 9.9 mm, a magnification of 1000×, and a standard probe current of 25. The surface morphology of the samples was visualized and recorded using the SEM system. Subsequent image analysis, including particle size measurements and surface structure evaluations, was conducted using ImageJ 1.54i version software.

2.6. Statistical Analysis

Calcium ion concentration data obtained from the AAS analysis were evaluated using a one-way Analysis of Variance (ANOVA) and followed by a Bonferroni post hoc test to identify statistically significant differences among the DBM-Ca(OH)₂ ratio groups. Other characterization parameters (XRD, FTIR, SEM-EDS) were analyzed descriptively by presenting their mean values. All statistical analyses were performed using the Statistical Package for the Social Sciences (SPSS 30) software for Windows, with the significance level set at $p < 0.05$.

3. Results

3.1. X-Ray Diffraction (XRD)

Figure 2 displays the XRD patterns of Ca(OH)_2 , DBM, and DBM- Ca(OH)_2 composites with varying ratios (1:1, 2:1, 3:1, and 4:1). The XRD pattern of pure Ca(OH)_2 shows distinct diffraction peaks at 2θ values around 17.9° , 28.5° , 34.0° , 47.0° , 50.7° , 54.2° , 62.5° , 64.1° , 71.6° , and 84.6° , which are consistent with its known crystalline structure. These peaks were also observed in the DBM- Ca(OH)_2 composite groups, indicating the presence of crystalline calcium hydroxide in these mixtures.

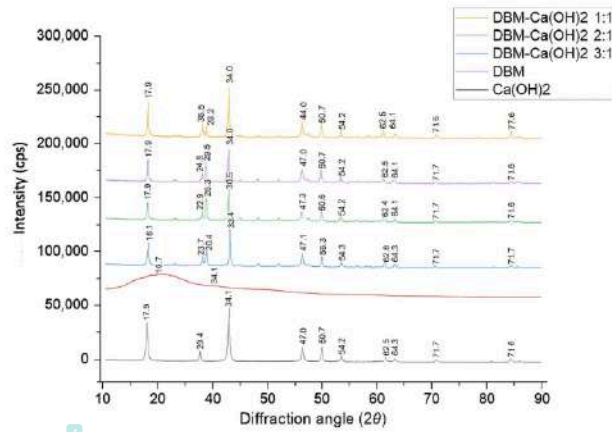


Figure 2. XRD spectra of DBM, Ca(OH)_2 , and DBM- Ca(OH)_2 composites in ratios of 1:1, 2:1, 3:1, 4:1.

The DBM sample exhibited an amorphous pattern with no distinct peaks, confirming the absence of crystalline phases after its demineralization. As the proportion of DBM increased (from 1:1 to 4:1), the intensity of the Ca(OH)_2 peaks gradually decreased, suggesting a reduced crystallinity due to dilution by the amorphous DBM.

Quantitative analysis of the degree of crystallinity showed the highest crystallinity in pure Ca(OH)_2 (63.1%), followed by DBM- Ca(OH)_2 at a 1:1 ratio (58.6%). The crystallinity progressively decreased to 48.1% in the 4:1 group (Table 1). These results indicate that increasing the DBM content attenuates the crystalline structure of Ca(OH)_2 in the composite, potentially enhancing the composite's bioresorbability and biological performance.

Table 1. Crystal phase and degree of crystallinity (%) of each sample, determined from XRD data.

Sample *	Crystal Phase	Degree of Crystallinity
DBM- Ca(OH)_2 1:1	Ca(OH)_2	58.6%
DBM- Ca(OH)_2 2:1	Ca(OH)_2	51.6%
DBM- Ca(OH)_2 3:1	Ca(OH)_2	48.5%
DBM- Ca(OH)_2 4:1	Ca(OH)_2	48.1%
DBM	-	-
Ca(OH)_2	Ca(OH)_2	63.1%

* One sample from each group was used for this test.

3.2. Atomic Absorption Spectroscopy (AAS)

The calcium ion release profile of Ca(OH)_2 , DBM, and the DBM- Ca(OH)_2 composites was evaluated using AAS after 7 days of incubation in Tris-HCl buffer (pH 7.4). The results, presented in Table 2, show a clear trend: the calcium ion concentration decreased with increasing proportions of DBM in the composite.

Table 2. Calcium ion concentration (mg/L) of Ca(OH)_2 , DBM, and DBM- Ca(OH)_2 composites, measured by AAS after 7 days of incubation in Tris-HCl buffer.

Sample	Number of Sample	Calcium Ion Concentration (mg/L) ($\bar{x} \pm \text{SD}$)	p-Value
DBM- Ca(OH)_2 1:1	3	218.56 \pm 1.37	<0.001*
DBM- Ca(OH)_2 2:1	3	214.71 \pm 1.53	
DBM- Ca(OH)_2 3:1	3	209.65 \pm 0.80	
DBM- Ca(OH)_2 4:1	3	205.11 \pm 0.99	
DBM	3	2.31 \pm 0.32	
Ca(OH)_2	3	229.60 \pm 1.94	

* There is a significant difference in the one-way ANOVA ($p < 0.05$).

The largest calcium ion release was observed in pure Ca(OH)_2 (229.60 \pm 1.94 mg/L), followed by DBM- Ca(OH)_2 composites in decreasing order: 1:1 (218.56 \pm 1.37 mg/L), 2:1 (214.71 \pm 1.53 mg/L), 3:1 (209.65 \pm 0.80 mg/L), and 4:1 (205.11 \pm 0.99 mg/L). DBM alone released a minimal amount of calcium ions (2.31 \pm 0.32 mg/L), confirming its demineralized state.

The one-way ANOVA revealed a statistically significant difference in calcium ion concentration among the groups ($p < 0.001$), with the DBM- Ca(OH)_2 4:1 group showing the lowest calcium release among the composites. This suggests that increasing the proportion of DBM dilutes the calcium content of the composite and reduces its ion release capacity.

3.3. Fourier Transform Infrared (FTIR) Spectroscopy

The FTIR spectra of DBM, Ca(OH)_2 , and the DBM- Ca(OH)_2 composites at ratios of 1:1, 2:1, 3:1, and 4:1 are shown in Figure 3 and Table 3. These spectra illustrate the characteristic functional groups of each material and confirm the presence of both organic and inorganic phases in the composites. In the DBM sample, the following characteristic peaks of collagen were observed:

- Amide A (N-H stretching) at 3595 cm^{-1} ;
- Amide B (C-H stretching) at 2924 cm^{-1} ;
- Amide I (C=O stretching) at 1634 cm^{-1} ;
- Amide II (N-H bending) at 1547 cm^{-1} ;
- Amide III (C-N stretching) at 1240 cm^{-1} ;
- OH^- at 3300 cm^{-1} .

The Ca(OH)_2 sample exhibited

OH^- stretching at 3641 cm^{-1} ;

CO_3^{2-} peak at 1463 cm^{-1} .

In the DBM- Ca(OH)_2 composites, notable new absorption bands confirmed the successful integration of inorganic content:

- PO_4^{3-} was detected at ~1056 cm^{-1} (1057 cm^{-1} in 3:1 group);
- COO^- bands were observed in the ranges of 1407–1417 cm^{-1} and 1641–1648 cm^{-1} across all composite groups, suggesting ionic interaction between Ca^{2+} and the carboxyl groups in collagen;
- OH^- stretching was present at 3638–3639 cm^{-1} in all composites.

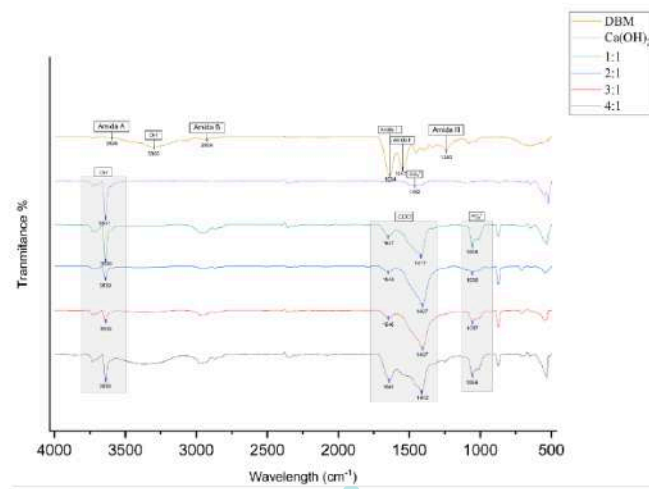


Figure 3. FTIR results for DBM, Ca(OH)_2 , and DBM- Ca(OH)_2 in ratios of 1:1, 2:1, 3:1, and 4:1. One sample from each group was used for this test.

Table 3. Absorption peaks of functional groups from the amide I, amide II, amide III, amide A, amide B, phosphate (PO_4^{3-}), carbonate (CO_3^{2-}), carboxylate (COO^-), and hydroxyl (OH^-) groups were detected.

Compound	Functional Group	Infrared Wavelength
Amide I	Stretching C=O	1600–1700 cm^{-1}
Amide II	Stretching C-N Bending N-H	1480–1575 cm^{-1}
Amide III	Stretching C-N Bending N-H	1200–1300 cm^{-1}
Amide A	Stretching N-H	3300–3500 cm^{-1}
Amide B	Stretching N-H	2900–3100 cm^{-1}
PO_4^{3-}	Asymmetry Stretching P-O	1030–1090 cm^{-1}
CO_3^{2-}	Asymmetry Stretching C-O	1400–1500 cm^{-1}
COO^-	Symmetry Stretching C-O-O	1300–1420 cm^{-1}
OH^-	Asymmetry Stretching C-O-O Stretching O-H	1550–1650 cm^{-1} 3300–3650 cm^{-1}

Characteristic collagen peaks from DBM (amide groups and hydroxyl) and mineral peaks from Ca(OH)_2 (hydroxyl and carbonate) are present in the composites, indicating the retention of both phases. Importantly, the appearance of phosphate (PO_4^{3-}) and carboxylate (COO^-) bands, along with shifts in hydroxyl stretching frequencies, demonstrates that chemical bonding and ionic interactions occur between the calcium ions and collagen carboxyl groups. These spectral changes suggest the formation of a bone-like apatite structure within the composite, which likely enhances its osteoconductive potential and suitability for bone regeneration applications.

3.4. Scanning Electron Microscope (SEM)—Energy-Dispersive X-Ray Spectroscopy (EDS)

The SEM micrographs of DBM, Ca(OH)_2 , and the DBM- Ca(OH)_2 composites with ratios of 1:1, 2:1, 3:1, and 4:1 are presented in Figure 4. Their visual appearance reveals the morphological differences among the samples, with Ca(OH)_2 particles exhibiting a broad size distribution. The DBM particles, being primarily organic, did not display distinct particulate features suitable for size measurements.

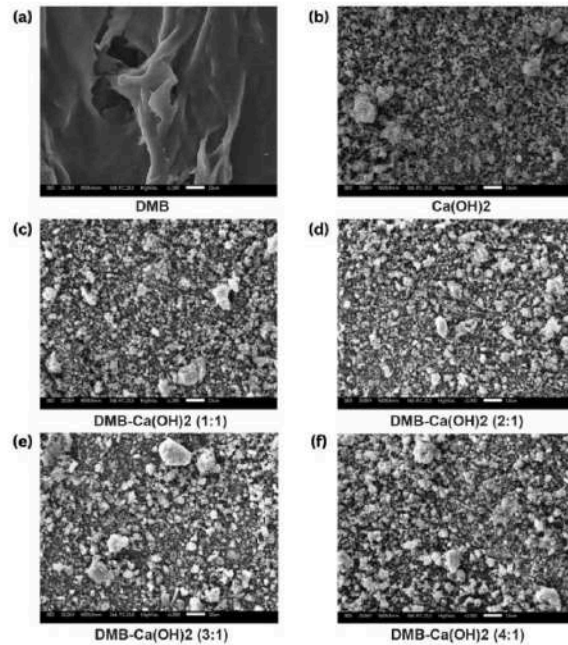


Figure 4. (a–f) The morphological characteristics of DBM- Ca(OH)_2 (1000 \times magnification).

The Ca(OH)_2 particles ranged from 0.01 μm to 350.68 μm in size, with an average particle size of $6.34 \pm 29.56 \mu\text{m}$. The incorporation of DBM into the composites reduced the maximum particle size and average particle size compared to pure Ca(OH)_2 . Specifically, average particle sizes decreased to $4.37 \pm 13.42 \mu\text{m}$ for the 1:1 ratio, $4.50 \pm 13.28 \mu\text{m}$ for 2:1, $3.65 \pm 9.35 \mu\text{m}$ for 3:1, and only slightly increased to $5.00 \pm 15.49 \mu\text{m}$ for 4:1. This trend suggests that the DBM addition influenced particle agglomeration and dispersion within the composites (Table 4).

The elemental composition of each sample was analyzed using EDS, with the spectra shown in Figure 5 and quantitative data detailed in Table 5. The primary elements detected across all samples include carbon (C), oxygen (O), sodium (Na), magnesium (Mg), aluminum (Al), chlorine (Cl), and calcium (Ca).

Table 4. Particle size distribution of Ca(OH)_2 and DBM- Ca(OH)_2 composites of different ratios, measured by SEM.

Sampl	Smallest Particle (μm)	Largest Particle (μm)	Average Particle Size (μm)	$\bar{x} \pm \text{SD}$
DBM *	-	-	-	-
Ca(OH)_2	0.01	350.68	6.34	6.34 ± 29.56
DBM- Ca(OH)_2 1:1	0.01	248.38	4.37	4.37 ± 13.42
DBM- Ca(OH)_2 2:1	0.01	149.67	4.50	4.50 ± 13.28
DBM- Ca(OH)_2 3:1	0.01	146.75	3.65	3.65 ± 9.35
DBM- Ca(OH)_2 4:1	0.01	197.28	5.00	5.00 ± 15.49

* Particle size measurements was not feasible for pure DBM. One sample from each group was used for this test.

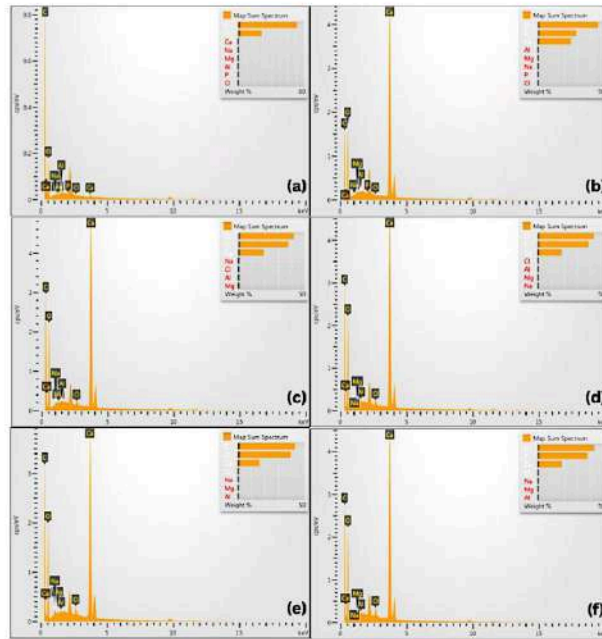


Figure 5. The Energy-Dispersive X-ray Spectroscopy (EDS) test results and the samples' composition: (a) DBM; (b) Ca(OH)_2 ; (c) DBM- Ca(OH)_2 1:1; (d) DBM- Ca(OH)_2 2:1; (e) DBM- Ca(OH)_2 3:1; (f) DBM- Ca(OH)_2 4:1.

In the pure DBM, carbon was the dominant element (71.14 wt%), reflecting the organic collagen in the matrix, with oxygen present at 28.51 wt%. In contrast, pure Ca(OH)_2 exhibited a higher oxygen content (45.55 wt%) and lower carbon content (29.04 wt%), consistent with its inorganic nature.

For DBM- Ca(OH)_2 composites, elemental compositions varied depending on their mixing ratio. Generally, their carbon and oxygen percentages shifted to intermediate values between those of pure DBM and Ca(OH)_2 , indicating the successful integration of

both components. Notably, the calcium content was maintained across the composites, supporting the presence of inorganic mineral phases critical for osteoconductivity, which contribute to the mechanical strength and stiffness of bone tissue. Phosphorus enhances the structural integrity and stability of bone. Carbon has been shown to promote the proliferation and differentiation of bone-forming cells within newly developing tissue. Meanwhile, oxygen facilitates the process of angiogenesis, which is essential for delivering nutrients and oxygen to the fracture site during the healing process.

These findings demonstrate the coexistence and homogeneous distribution of organic (DBM) and inorganic (Ca(OH)_2) phases within the composites, which may enhance their biological and mechanical properties for bone regeneration applications.

Table 5. Elemental composition (weight percentage) of DBM, Ca(OH)_2 , and DBM- Ca(OH)_2 composites, measured by ED6.

Element	DBM	Ca(OH)_2	DBM- Ca(OH)_2 1:1	DBM- Ca(OH)_2 2:1	DBM- Ca(OH)_2 3:1	DBM- Ca(OH)_2 4:1
	Wt%	Wt%	Wt%	Wt%	Wt%	Wt%
C	71.14	29.04	37.7	38.47	42.89	37.60
O	28.51	45.55	42.13	42.35	39.66	42.70
Na	0	0	0.28	0.21	0.48	0.52
Mg	0	0.23	0.14	0.23	0.16	0.20
Al	0	0.24	0.2	0.23	0.15	0.19
Cl	0	0	0.25	0.31	0.53	0.6
Ca	0.35	24.94	19.3	18.2	16.12	18.2

One sample from each group was used for this test.

4. Discussion

This study explored the physicochemical and morphological properties of DBM- Ca(OH)_2 composites with varying ratios to evaluate their potential as bone graft materials. Each analytical technique—XRD, AAS, FTIR, and SEM—provided valuable insights into how the combination of DBM- Ca(OH)_2 influences structural, chemical, and surface characteristics that are critical for bone regeneration.

XRD analysis revealed important information about the crystallinity and phase composition of the composites. Pure Ca(OH)_2 exhibited sharp and distinct diffraction peaks, which correspond to its well-ordered crystalline structure. These peaks serve as fingerprints confirming the presence of highly crystalline Ca(OH)_2 . When DBM was added to the composite in increasing proportions, the intensity of these crystalline peaks diminished noticeably. This decrease indicates a reduction in crystallinity due to the incorporation of DBM, which is predominantly amorphous and composed mainly of collagen and organic matrix components. The highest DBM ratio (4:1) showed the lowest peak intensity, suggesting that the amorphous phase of DBM increasingly disrupted the ordered crystalline lattice of calcium hydroxide.

The degree of crystallinity is a key factor influencing a material's behavior in biological environments. Lower crystallinity tends to enhance bioactivity by improving cell adhesion and accelerating degradation, which facilitates the natural bone remodeling process [31,32]. However, highly amorphous materials may lack sufficient mechanical strength to support this process. In this context, the 2:1 DBM- Ca(OH)_2 composite exhibited moderate crystallinity, indicating a promising balance between maintaining enough structural integrity and providing an active surface favorable for osteoblast function [33]. This suggests that tuning the DBM-to- Ca(OH)_2 ratio can modulate crystallinity and thus tailor the composite's performance to specific clinical needs.

Calcium ion release, as measured by AAS, is a crucial parameter because calcium ions regulate multiple cellular processes essential for bone formation, including osteoblast proliferation, differentiation, and mineralization [34,35]. The results showed that pure $\text{Ca}(\text{OH})_2$ released the largest amount of calcium ions, reflecting its high solubility. Conversely, DBM released minimal calcium due to its largely organic, demineralized nature. Composite samples exhibited calcium release levels inversely proportional to their DBM content; as the amount of DBM present increased, calcium release decreased significantly [36–38].

Maintaining calcium ion release within an optimal physiological range is essential because while calcium is necessary for bone healing, excessive calcium concentrations can be cytotoxic to osteoblasts [39–41]. The ideal range for promoting osteogenic activity is generally between 60 and 90 mg/L. In this study, all composite formulations exceeded this range, but the DBM- $\text{Ca}(\text{OH})_2$ composite (ratio 4:1) released the lowest calcium concentration, suggesting a more controlled release profile that might reduce potential cytotoxicity while still supporting bone regeneration. The DBM- $\text{Ca}(\text{OH})_2$ composite created at a 2:1 ratio released higher levels of calcium, which could accelerate osteoblast activity and bone formation but might also increase the risk of cellular stress if concentrations become excessive. These findings highlight the importance of optimizing the composite's formulation to balance calcium availability with biological safety and efficacy.

The decreasing amount of calcium ion released with the increasing DBM content can be explained by the presence of collagen-rich, amorphous DBM, which reduces overall solubility and slows the diffusion of calcium ions from the composite. This slower and more sustained release may be advantageous for long-term bone healing, providing a steady supply of calcium ions that supports gradual mineralization without overwhelming the cellular environment [42]. In contrast, composites with lower DBM contents may degrade faster, releasing calcium ions rapidly but risking cytotoxicity and impaired osteoblast function [43]. Thus, both the 4:1 and 2:1 composites represent viable options, with the former offering safer, sustained release and the latter favoring faster bone regeneration.

Our FTIR analysis further clarified the chemical composition and molecular interactions within the composites. The DBM control exhibited characteristic absorption bands associated with amide groups (amide I, II, III, A, and B), confirming the presence of collagen, the primary organic component of bone matrix responsible for structural support and cell signaling [44,45]. In contrast, the $\text{Ca}(\text{OH})_2$ (as control) displayed strong peaks related to hydroxyl and carbonate groups, consistent with its inorganic mineral composition and high alkalinity [46,47].

In the DBM- $\text{Ca}(\text{OH})_2$ composites, the typical amide bands of collagen were diminished or absent, while phosphate and carboxylate ion peaks became more prominent [48,49]. This indicates that chemical changes occurred during composite preparation, likely due to hydrolysis reactions caused by the alkaline environment from the $\text{Ca}(\text{OH})_2$. These reactions may break the peptide bonds in collagen, generating carboxylate-containing groups and altering the organic matrix's structure [50–52]. The presence of phosphate bands suggests that residual mineral components remain within the composite despite the demineralization process. These phosphate groups could enhance osteoconductivity by supporting mineral deposition during bone formation. Understanding these molecular-level changes is vital because they influence both the mechanical properties and the biological responses elicited by the composite graft.

SEM provided critical morphological data, revealing how surface texture, particle size, and shape affect the composite's interaction with cells and its overall bioactivity [53–55]. Rough surface structures were observed, particularly in the DBM- $\text{Ca}(\text{OH})_2$ composite (ratio 4:1), consistent with previous studies demonstrating that roughness enhances protein

adsorption and promotes osteoblast attachment, proliferation, and differentiation [56,57]. These factors are essential for effective osseointegration and bone regeneration.

Particle size also influences the biological response. Although the literature often cites particles of around 100 μm as optimal for osteoblast activation [28], the microparticle size observed in the composites ($\sim 5 \mu\text{m}$) falls within a size range shown to positively affect bone growth factors and increase the surface area available for cellular interactions. Smaller particles may also improve resorbability, allowing the graft to be gradually replaced by new bone tissue.

Regarding particle shape, $\text{Ca}(\text{OH})_2$ typically appears as small granular or blocky particles, while DBM forms flake-like fragments [58,59]. In the DBM- $\text{Ca}(\text{OH})_2$ composite, particle morphology became more uniform and denser, especially at the 4:1 ratio. This denser particle arrangement likely facilitates mechanical interlocking and enhances cellular adhesion, both of which are beneficial for osteogenesis and graft stability [60,61]. Together, these morphological features reinforce the composite's suitability as a scaffold for bone healing.

In summary, the results demonstrate that increasing the amount of DBM in the DBM- $\text{Ca}(\text{OH})_2$ composite influences its crystallinity, calcium release profile, chemical composition, and surface morphology, all of which affect its biological performance. The 4:1 composite exhibits a lower crystallinity, controlled calcium ion release, chemically modified organic components, and an optimal surface morphology that collectively support sustained bone regeneration with potentially reduced cytotoxicity. The 2:1 composite maintains moderate crystallinity and releases higher concentrations of calcium, offering a balance between mechanical support and accelerated bioactivity.

Both composite formulations hold promise as bone graft materials. However, further biological studies, including cell cultures and *in vivo* bone regeneration models, are necessary to validate their osteogenic potential and optimize their ratios for specific clinical applications. In addition, further *in vitro* studies are recommended to assess the cytocompatibility of the ions released from the composites, which is critical for ensuring their safety and effectiveness in biological environments. This multiparametric characterization provides a solid foundation for designing bone graft substitutes with properties that are tailored to meet diverse therapeutic needs. Another limitation of this study is that the particle size, crystallinity, and elemental analyses were each conducted on a single sample per formulation. As such, statistical comparisons could not be performed; further replicates are recommended in future studies to ensure reproducibility and assess variability.

5. Conclusions

This study investigated the physicochemical and compositional characteristics of DBM- $\text{Ca}(\text{OH})_2$ composites with varying ratios to identify a formulation suitable for bone regeneration. Increasing the DBM content in the composite led to a reduction in crystallinity and calcium ion release, along with a modulation of particle size distribution. These changes reflect a shift toward a more bioresorbable and biologically responsive material.

Among the tested formulations, the 2:1 DBM- $\text{Ca}(\text{OH})_2$ ratio demonstrated an optimal balance. It maintained sufficient calcium availability to support osteogenic activity, exhibited a moderately reduced crystallinity conducive to biodegradation, and presented a favorable average particle size that may enhance cellular attachment and proliferation. The composite also retained the essential organic and inorganic functional groups from both components, suggesting successful integration and the potential for mineralized tissue formation. Overall, the DBM- $\text{Ca}(\text{OH})_2$ composite at a 2:1 ratio is a promising candidate for bone graft applications, offering a combination of structural support and biological functionality.

6. Patents

The work reported in this manuscript resulted in a patent granted by the Directorate General of Intellectual Property (DJKI) under the number EC00202517207.

Author Contributions: Conceptualization, O., F.L.K. and O.N.K.; methodology, O., F.L.K. and O.N.K.; software, F.A.L.; validation, O., F.L.K. and O.N.K.; formal analysis, F.A.L.; investigation, F.A.L.; resources, O., F.L.K. and O.N.K.; data curation, F.A.L.; writing—original draft preparation, F.A.L.; writing—review and editing, O., F.L.K., O.N.K. and M.D.C.S.; visualization, F.A.L. and M.D.C.S.; supervision, O., F.L.K. and O.N.K.; project administration, O., F.L.K. and O.N.K.; funding acquisition, O., F.L.K. and O.N.K. All authors have read and agreed to the published version of the manuscript.

Funding: This research was fully funded by Universitas Trisakti under contract number 360/A.1/LPPM-P/USAKTI/X/2024.

Institutional Review Board Statement: This study was approved by the Ethics Committee of Universitas Trisakti (783/S1/KEPK/FGK/6/2024, 14 June 2024, and 839/S1/KEPK/FGK/7/2024, 5 July 2024).

Data Availability Statement: The raw data supporting the conclusions of this article will be made available by the authors on request.

Conflicts of Interest: The authors declare no conflicts of interest.

References

1. Nibali, L.; Sultan, D.; Arena, C.; Pelekos, G.; Lin, G.; Tonetti, M. Periodontal infrabony defects: Systematic review of healing by defect morphology following regenerative surgery. *J. Clin. Periodontol.* **2021**, *48*, 100–113. [[CrossRef](#)] [[PubMed](#)]
2. Tsuchida, S.; Nakayama, T. Recent clinical treatment and basic research on the alveolar bone. *Biomedicines* **2023**, *11*, 843. [[CrossRef](#)] [[PubMed](#)]
3. Boehm, T.K.; Clara, S.K. *An Overview of Periodontal Surgical Procedures*; StatPearls Publishing: Treasure Island, FL, USA, 2024.
4. Ciszynski, M.; Dominiak, S.; Dominiak, M.; Gedrange, T.; Hadzik, J. Allogenic bone graft in dentistry: A review of current trends and developments. *Int. J. Mol. Sci.* **2023**, *24*, 16598. [[CrossRef](#)]
5. Zhang, X.; Li, Q.; Wang, Z.; Zhou, W.; Zhang, L.; Liu, Y.; Xu, Z.; Li, Z.; Zhu, C.; Zhang, X. Bone regeneration materials and their application over 20 years: A bibliometric study and systematic review. *Front. Bioeng. Biotechnol.* **2022**, *10*, 921092. [[CrossRef](#)]
6. Wibowo, A.R.; Octarina, O.; Munadzirah, E.; Handharyani, E. The effect of application bovine amniotic membrane on osteoblasts, osteocytes, and collagen. *Padjadjaran J. Dent.* **2023**, *35*, 163–169. [[CrossRef](#)]
7. Veremeev, A.; Bolgarin, R.; Nesterenko, V.; Andreev-Andrievskiy, A.; Kutikhin, A. Native bovine hydroxyapatite powder, demineralised bone matrix powder, and purified bone collagen membranes are efficient in repair of critical-sized rat calvarial defects. *Materials* **2020**, *13*, 3393. [[CrossRef](#)]
8. Zhang, H.; Yang, L.; Yang, X.-G.; Wang, F.; Feng, J.; Hua, K.; Li, Q.; Hu, Y. Demineralized bone matrix carriers and their clinical applications: An overview. *Orthop. Surg.* **2019**, *11*, 725–737. [[CrossRef](#)] [[PubMed](#)]
9. Chen, L.-C.; Su, C.-Y.; Lai, C.-C.; Tsou, Y.-S.; Zheng, Y.; Fang, H.-W. Preparation and characterization of moldable demineralized bone matrix/calcium sulfate composite bone graft materials. *J. Funct. Biomater.* **2021**, *12*, 56. [[CrossRef](#)] [[PubMed](#)]
10. Wen, B.; Freilich, M.; Kuhn, L. Bone Tissue Engineering Around Dental Implants. *Stem Cell Biol. Tissue Eng. Dent. Sci.* **2015**, *55*, 749–764.
11. Cho, H.; Bucciarelli, A.; Kim, W.; Jeong, Y. Natural Sources and Applications of Demineralized Bone Matrix in the Field of Bone and Cartilage Tissue Engineering. *Adv. Exp. Med. Biol.* **2020**, *1249*, 3–14.
12. Sawkins, M.; Bowen, W.; Dhadha, P.; Markides, H.; Sidney, L.; Taylor, A.; Rose, F.; Badylak, S.; Shakesheff, K.; White, L. Hydrogels derived from demineralized and decellularized bone extracellular matrix. *Acta Biomater.* **2013**, *9*, 7865–7873. [[CrossRef](#)] [[PubMed](#)]
13. Verboket, R.D.; Irrle, T.; Busche, Y.; Schaible, A.; Schröder, K.; Brune, J.C.; Marzi, I.; Nau, C.; Henrich, D. Fibrous demineralized bone matrix (DBM) improves bone marrow mononuclear cell (BMC)-supported bone healing in large femoral bone defects in rats. *Cells* **2021**, *10*, 1249. [[CrossRef](#)] [[PubMed](#)]
14. Khosropanah, H.; Lashkarizadeh, N.; Ayatollahi, M.; Kaviani, M.; Mostafavipour, Z. The impact of calcium hydroxide on the osteoinductive capacity of demineralized freeze-dried bone allograft: An in-vitro study. *J. Dent. Shiraz. Univ. Med. Sci.* **2018**, *19*, 19–27.
15. Mahajan, A.; Kedige, S. Periodontal bone regeneration in intrabony defects using osteoconductive bone graft versus combination of osteoconductive and osteostimulative bone graft: A comparative study. *J. Dent. Res.* **2015**, *12*, 25–30. [[CrossRef](#)]

16. Khorshidi, H.; Raofifi, S.; Sabagh, S.; Behboud, Z.; Mozafari, G.; Ashraf, M. Effect of combined calcium hydroxide and accelerated portland cement on bone formation and soft tissue healing in dog bone lesions. *J. Dent. Biomater.* **2015**, *2*, 97–102.
17. Dhruvakumar, D.; Gupta, C. Role of combination therapy/composite graft in periodontal regeneration: A mini review. *Tanta Dent. J.* **2017**, *14*, 169. [CrossRef]
18. Barus, L.; Septianingtyas, V.; Febriadi, P.B.; Hendra, I.M.; Annis, A.F.; Satria, R.M.H.; Wibisono, N.I.; Pratiwi, E.S.; Rasyida, A.Z.; Mulyawan, I.; et al. Demineralized Freeze-Dried Bovine Bone Xenograft Granules as Alveolar Bone Substitutes: A Profile Study. 2021. Available online: <http://www.ijidmr.com> (accessed on 8 June 2025).
19. Coathup, M.; Campion, C.; Blunn, G. A carboxymethyl cellulose bone graft carrier delays early bone healing in an ovine model. *J. Biomed. Mater. Res.-Part B Appl. Biomater.* **2020**, *108*, 612–618. [CrossRef]
20. Chauhan, N.; Lakkhar, N.; Chaudhari, A. Development and physicochemical characterization of novel porous phosphate glass bone graft substitute and in vitro comparison with xenograft. *J. Mater. Sci. Mater. Med.* **2021**, *32*, 60. [CrossRef]
21. Kurniawan, F.L.; Tjandrawinata, R.; Marpaung, C.; Pratiwi, D.; Komariah, K. The effect of horn beetle nanochitosan (*Xylotrupes gideon*) addition on the hardness of glass-ionomer cement. *J. Indones. Dent. Assoc.* **2022**, *5*, 27–31. [CrossRef]
22. Livia, F.; Tjandrawinata, R.; Marpaung, C.D.; Pratiwi, D.; Komariah, K. The effect of horn beetle nano chitosan (*Xylotrupes gideon*) on the surface roughness of glass-ionomer cement. *Mater. Sci. Forum.* **2022**, *1069*, 161–166. [CrossRef]
23. Ali, A.; Chiang, Y.W.; Santos, R.M. X-ray diffraction techniques for mineral characterization: A review for engineers of the fundamentals, applications, and research directions. *Minerals* **2022**, *12*, 205. [CrossRef]
24. Khan, H.; Yerramilli, A.S.; D'Oliveira, A.; Alford, T.L.; Boffito, D.C.; Patience, G.S. Experimental methods in chemical engineering: X-ray diffraction spectroscopy—XRD. *Can. J. Chem. Eng.* **2020**, *98*, 1255–1266. [CrossRef]
25. Filio, P.; Octarina, F.; Komariah, F. Characterization of fabricated bovine hydroxyapatite crystal as socket preservation material: An SEM-EDX and x-ray diffraction study. *World J. Dent.* **2022**, *13* (Suppl. S2), S175–S181. [CrossRef]
26. Filho, H.J.I.; Salazar, R.F.S.; Capri, M.R.; Neto, A.C.; Alcantara, M.A.K.; Peixoto, A.L.C. State-of-the-art and trends in atomic absorption spectrometry. In *Atomic Absorption Spectroscopy*; InTech: Houston, TX, USA, 2012; pp. 13–36.
27. Berna, F. *Encyclopedia of Geoarchaeology*; Springer: Dordrecht, The Netherlands, 2017.
28. Nam, J.-W.; Kim, M.-Y.; Han, S.-J. Cranial Bone Regeneration According to Different Particle Sizes and Densities of Demineralized Dentin Matrix in The Rabbit Model. *Maxillofac. Plast. Reconstr. Surg.* **2016**, *38*, 27. [CrossRef]
29. Charlena, C.; Maddu, A.; Hidayat, T. Synthesis and Characterization of hydroxyapatite from green mussel shell with sol-gel method. *J. Kim. Val.* **2022**, *8*, 269–279. [CrossRef]
30. Widjonarko, N.E. Introduction to advanced x-ray diffraction techniques for polymeric thin films. *Coatings* **2016**, *6*, 54. [CrossRef]
31. Dozza, B.; Lesci, I.G.; Duchi, S.; Della Bella, E.; Martini, L.; Salamanna, F.; Falconi, M.; Cinotti, S.; Fini, M.; Lucarelli, E.; et al. When size matters: Differences in demineralized bone matrix particles affect collagen structure, mesenchymal stem cell behaviour, and osteogenic potential. *J. Biomed. Mater. Res.* **2017**, *105*, 1019–1033. [CrossRef]
32. Nicoletti, A.; Torricelli, P.; Bigi, A.; Fornasari, P.; Fini, M.; Moroni, L. Incorporation of nanostructured hydroxyapatite and poly(*N*-isopropylacrylamide) in demineralized bone matrix enhances osteoblast and human mesenchymal stem cell activity. *Biomaterphases* **2015**, *10*, 041001. [CrossRef]
33. Chacón, V.P.G.; Habibovic, P. Deconvoluting the bioactivity of calcium phosphate-based bone graft substitutes: Strategies to understand the role of individual material properties. *Adv. Healthc. Mater.* **2017**, *6*, 1601478. [CrossRef]
34. Mohammadi, M.; Shaegh, S.A.M.; Alibolandi, M.; Ebrahimpzadeh, M.H.; Tamayol, A.; Jaafari, M.R.; Ramezani, M. Micro and nanotechnologies for bone regeneration: Recent advances and emerging designs. *J. Control. Release* **2018**, *274*, 35–55. [CrossRef]
35. Manalu, J.L.; Soegijono, B.; Indrani, D.J. Characterization of hydroxyapatite derived from bovine bone. *Asian J. Appl. Sci.* **2015**, *3*, 758–765.
36. Ovrebo, O.; Orlando, L.; Rubenis, K.; Ciriello, L.; Ma, Q.; Giorgi, Z.; Tognoni, S.; Loca, D.; Villa, T.; Nogueira, L.P.; et al. The role of collagen and crystallinity in the physicochemical properties of naturally derived bone grafts. *Regen. Biomater.* **2024**, *11*, rbae093. [CrossRef] [PubMed]
37. Hong, K. Analysis of crystal structure of bone graft material using analyses of x-Ray diffraction and scanning electron microscope image. *Int. J. Clin. Prev. Dent.* **2019**, *15*, 215–219. [CrossRef]
38. Park, M.; Mah, Y.J.; Kim, D.H.; Kim, E.S.; Park, E.J. Demineralized deciduous tooth as a source of bone graft material: Its biological and physicochemical characteristics. *Oral Surg. Oral Med. Oral Pathol. Oral Radiol.* **2015**, *120*, 307–314. [CrossRef]
39. Haugen, H.J.; Lyngstadnaas, S.P.; Rossi, F.; Perale, G. Bone grafts: Which is the ideal biomaterial. *J. Clin. Periodontol.* **2019**, *46* (Suppl. S21), 92–102. [CrossRef]
40. Montazerian, M.; Shearer, A.; Mauro, J.C. Perspectives on the impact of crystallization in bioactive glasses and glass-ceramics. *Int. J. Ceram. Eng. Sci.* **2023**, *6*, e10194. [CrossRef]
41. Kuzmenka, D.; Sewohl, C.; König, A.; Flath, T.; Hahnel, S.; Schulze, F.P.; Hacker, M.C.; Schulz-Siegmund, M. Sustained calcium(II)-release to impart bioactivity in hybrid glass scaffolds for bone tissue engineering. *Pharmaceutics* **2020**, *12*, 1192. [CrossRef]

42. Berberi, A.; Samarani, A.; Nader, N.; Noujeim, Z.; Dagher, M.; Kanj, W.; Mearawi, R.; Saleme, Z.; Badran, B. Physicochemical characteristics of bone substitutes used in oral surgery in comparison to autogenous bone. *BioMed Res. Int.* **2014**, *2014*, 320790. [CrossRef]
43. Sunarso; Rahmawati, D.; Irawan, B.; Pangesty, A.I. A novel method to fabricate monetite granules for bone graft applications. *Dent. Mater. J.* **2024**, *43*, 67–73. [CrossRef]
44. Roldan, L.; Isaza, C.; Ospina, J.; Montoya, C.; Domínguez, J.; Orrego, S.; Correa, S. A Comparative Study of HA/DBM Compounds Derived from Bovine and Porcine for Bone Regeneration. *J. Funct. Biomater.* **2023**, *14*, 439. [CrossRef]
45. Suptijah, P.; Indriani, D.; Wardoyo, S.E. Isolasi dan karakterisasi kolagen dari kulit ikan patin (*Pangasius sp.*). *J. Sains Nat.* **2018**, *8*, 8–23. [CrossRef]
46. Kiefer, J.; Stärk, A.; Kiefer, A.; Glade, H. Infrared Spectroscopic Analysis of the Inorganic Deposits from Water in Domestic and Technical Heat Exchangers. *Energies* **2018**, *11*, 798. [CrossRef]
47. Riaz, T.; Zeeshan, R.; Zarif, F.; Ilyas, K.; Muhammad, N.; Safi, S.Z.; Rahim, A.; Rizvi, S.A.A.; Rehman, I.U. FTIR analysis of natural and synthetic collagen. *Appl. Spectrosc. Rev.* **2018**, *53*, 703–746. [CrossRef]
48. Idiawati, N.; Novita, I.; Nurdiansyah, S.I.; Minsas, S.; Siregar, S. Identifikasi kolagen dari cangkang bulu babi (*Diadema setosum*) asal perairan Pulau Lemukutan. *Marinade* **2022**, *5*, 136–141. [CrossRef]
49. Sizeland, K.H.; Hofman, K.A.; Hallett, I.C.; Martin, D.E.; Potgieter, J.; Kirby, N.M.; Hawley, A.; Mudie, S.T.; Ryan, T.M.; Haverkamp, R.G.; et al. Nanostructure of electrospun collagen: Do electrospun collagen fibers form native structures? *Materialia* **2018**, *3*, 90–96. [CrossRef]
50. Hossain, M.S.; Ahmed, S. FTIR spectrum analysis to predict the crystalline and amorphous phases of hydroxyapatite: A comparison of vibrational motion to reflection. *RSC Adv.* **2023**, *13*, 14625–14630. [CrossRef]
51. Nandiyanto, A.B.D.; Oktiani, R.; Ragadhita, R. How to Read and Interpret FTIR Spectroscopy of Organic Material. *Indones. J. Sci. Technol.* **2019**, *4*, 97. [CrossRef]
52. Febri, W.; Astuti, E.; Trisnawati, P. Uji Hidrolisis Parasetamol dalam Larutan pH 2,0; 5,0; dan 7,0 Pada Suhu 37 °C. Bachelor's Thesis, Program Studi Farmasi, Fakultas Sains dan Teknologi, Universitas Peradaban, 2022. Available online: <http://repository.peradaban.ac.id/eprint/11076> (accessed on 8 June 2025).
53. Bariyah, N.; Pascawinata, A.; Firdaus, F. Gambaran Karakteristik Scaffold Hidroksiapatit Gigi Manusia Dengan Metode Planetary Ball Mill Menggunakan Uji Scanning Electron Microscope (Sem). *B-Dent. Kadokt. Gigi Univ. Baiturrahmah* **2016**, *3*, 131–138. [CrossRef]
54. Munadzirah, E.; Razak, F.A.; Abbas, B.; Soekartono, H.; Agustantina, T.H.; Surboyo, M.D. Characterization of bovine sponge amnion (BSA) by a novel process for dental treatment. *J. Int. Dent. Med. Res.* **2022**, *15*, 479–484.
55. O'Connor, D.; Sexton, B.; Smart, R. *Surface Analysis Methods in Materials Science*; Springer Series in Surface Sciences; Springer Nature: Dordrecht, The Netherlands, 2013.
56. Dewi, M.; Peornomo, H. The Effect of Zirconia Material for Dental Implant to Osseointegrated Process. *SONDE (Sound Dent.)* **2020**, *5*, 39–53. [CrossRef]
57. Le Guéhennec, L.; Soueidan, A.; Layrolle, P.; Amourig, Y. Surface treatments of titanium dental implants for rapid osseointegration. *Dent. Mater.* **2007**, *23*, 844–854. [CrossRef] [PubMed]
58. Engbrecht, D.C.; Hirschfeld, D. Thermal analysis of calcium sulfate dihydrate sources used to manufacture gypsum wallboard. *Thermochim. Acta* **2016**, *639*, 173–185. [CrossRef]
59. Grawish, M.E. Demineralized dentin matrix for dental and alveolar bone tissues regeneration: An innovative scope review. *Tissue Eng. Regen. Med.* **2022**, *19*, 687–701. [CrossRef] [PubMed]
60. Li, Q. Demineralized bone matrix-based microcarrier scaffold favors vascularized large bone regeneration in vivo in a rat model. *J. Biomater. Appl.* **2018**, *33*, 182–195. [CrossRef]
61. Leni, A.; Hariyani, N.A. Hidroksiapatit sebagai salah satu bahan yang paling umum digunakan pada cangkang tulang. *J. Kedokt. Gigi Univ. Baiturrahmah* **2021**, *8*, 172–178. [CrossRef]

Disclaimer/Publisher's Note: The statements, opinions and data contained in all publications are solely those of the individual author(s) and contributor(s) and not of MDPI and/or the editor(s). MDPI and/or the editor(s) disclaim responsibility for any injury to people or property resulting from any ideas, methods, instructions or products referred to in the content.

Physicochemical Properties of Demineralized Bone Matrix and Calcium Hydroxide Composites Used as Bone Graft Material

ORIGINALITY REPORT

10%

SIMILARITY INDEX

7%

INTERNET SOURCES

8%

PUBLICATIONS

6%

STUDENT PAPERS

PRIMARY SOURCES

1	id.123dok.com Internet Source	1%
2	Mohamed El Habib Hitar, Latifa Tajounte, Manal Benyoussef, Abdellah Benzaouak et al. "Influence of Manganese Addition on Structural, Dielectric, and Wastewater Bioconversion in LiTaO3 Ferroelectric Material", Crystals, 2025 Publication	1%
3	Submitted to George Mason University Student Paper	1%
4	Yunjun Wang. "Effect of Manganese Ions on the Structure of Ca(OH) ₂ and Mercury Adsorption Performance of Mn ^{x+} /Ca(OH) ₂ Composites", Energy & Fuels, 04/21/2011 Publication	1%
5	Adegbite Adesipo, Oluwaseun Fadeyi, Kamil Kuca, Ondrej Krejcar, Petra Maresova, Ali Selamat, Mayowa Adenola. "Smart and Climate-Smart Agricultural Trends as Core Aspects of Smart Village Functions", Sensors, 2020 Publication	1%
6	www.karyailmiah.trisakti.ac.id Internet Source	1%
7	www.preprints.org Internet Source	1%
8	Submitted to University of Leeds	

1 %

9 pubs.rsc.org
Internet Source <1 %

10 mts.intechopen.com
Internet Source <1 %

11 www.hilarispublisher.com
Internet Source <1 %

12 Submitted to Fakultas Teknologi Kebumian dan Energi Universitas Trisakti
Student Paper <1 %

13 iv.iiarjournals.org
Internet Source <1 %

14 eprints.whiterose.ac.uk
Internet Source <1 %

15 journals.e-palli.com
Internet Source <1 %

16 Adrian Ionuț Nicoară, Vlad Cocoș, Cristina Chircov, Roxana Doina Trușcă, Ariana Hudiță. "3D-printed poly-ε-caprolactone/bioglass and iron disulfide composite materials for hard tissue engineering", *Ceramics International*, 2025
Publication <1 %

17 Submitted to Uganda Christian University
Student Paper <1 %

18 re.public.polimi.it
Internet Source <1 %

19 Submitted to Saginaw Valley State University
Student Paper <1 %

20 Yunjun Wang, Yufeng Duan. " Effect of Manganese Ions on the Structure of Ca(OH) and Mercury Adsorption Performance of Mn /Ca(OH) Composites ", *Energy & Fuels*, 2011
Publication <1 %

21

discovery.dundee.ac.uk

Internet Source

<1%

Exclude quotes On

Exclude matches < 15 words

Exclude bibliography On

[Crystals] Manuscript ID: crystals-3620443 - Accepted for Publication

1 message

Crystals Editorial Office <crystals@mdpi.com>

Mon, Jun 9, 2025 at 2:40 PM

Reply-To: Natrawee Khetwunchai <khetwunchai@mdpi.com>, Crystals Editorial Office <crystals@mdpi.com>

To: Florencia Livia Kurniawan <florencia@trisakti.ac.id>, Meircurius Dwi Condro Surboyo <meircurius-2015@fkg.unair.ac.id>

Cc: Octarina Octarina <octarina@trisakti.ac.id>, Firda Amalia Larosa <famalia02@gmail.com>, Olivia Nauli Komala <olivia.nauli@trisakti.ac.id>, Crystals Editorial Office <crystals@mdpi.com>, Natrawee Khetwunchai <khetwunchai@mdpi.com>

Dear Dr. Kurniawan,

Congratulations on the acceptance of your manuscript, and thank you for submitting your work to Crystals. Please see the relevant manuscript details below:

Manuscript ID: crystals-3620443

Type of manuscript: Article

Title: Properties of Demineralized Bone Matrix Combined with Calcium as a Bone Graft Candidate

Authors: Octarina Octarina, Florencia Livia Kurniawan *, Firda Amalia Larosa, Olivia Nauli Komala, Meircurius Dwi Condro Surboyo

Received: 16 Apr 2025

E-mails: octarina@trisakti.ac.id, florencia@trisakti.ac.id, famalia02@gmail.com, olivia.nauli@trisakti.ac.id, meircurius-2015@fkg.unair.ac.id

https://susy.mdpi.com/user/manuscripts/review_info/57afeb1ad58af2ea6fa6fc028b6773e0

We will now edit your paper; once complete, we will return it to you for your review and approval. Within the next few days, an invoice for the article processing charge (APC), required for publication, will be sent by email from the Editorial Office in Basel, Switzerland.

If, however, your manuscript requires extensive English language and grammar revisions, we will need to return the paper and request that such changes are made.

We encourage you to set up a profile on SciProfiles.com, MDPI's researcher network platform. Articles you publish with MDPI will be linked to your SciProfiles page, where your colleagues and peers will be able to see all of your publications, citations, and other academic contributions.

Kind regards,
Alessandra Toncelli
Editor-in-Chief